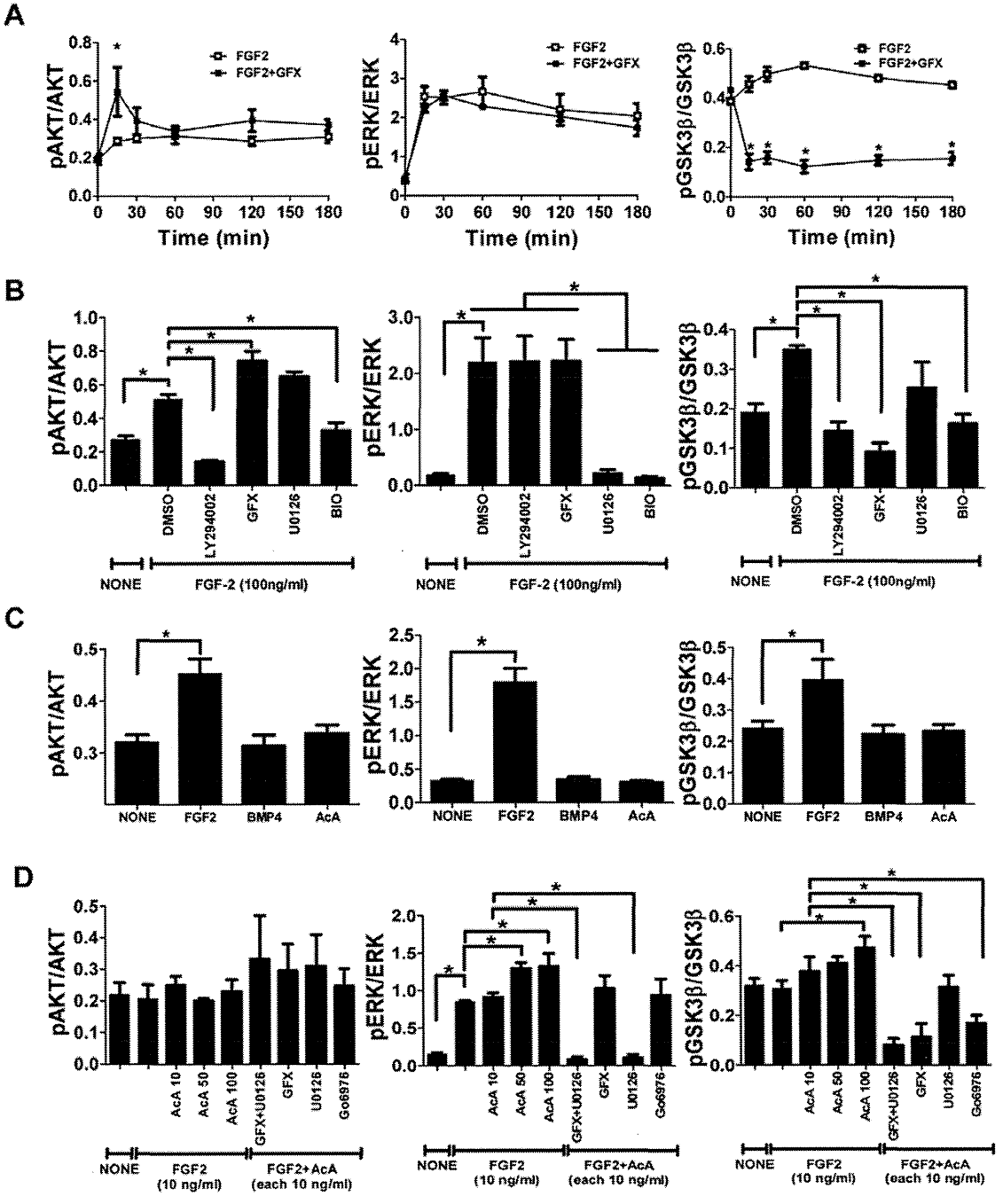

Figure 2. Effect of PKC inhibitor on FGF-2 signaling in hPS cells. The phosphorylation levels in H9 hES cells were measured by AlphaScreen® SureFire® assay kit. The values of the y-axis are the ratio of each phosphorylation to each total signal protein. (A) The cells were stimulated with FGF-2 (100 ng/ml) in fresh medium without insulin after overnight starvation and incubated with (open square) or without GFX (5 μM, closed square) for 180 minutes. The data are represented as means ± SE (n = 3). *P<0.05. (B) The cells were stimulated with FGF-2 (100 ng/ml) in fresh medium without insulin after overnight starvation. Fifteen minutes after FGF-2 addition together with each inhibitor as indicated on the panel. The data are represented as means ± SE (n = 3). *P<0.05. (C) The cells were treated with FGF-2 (100 ng/ml), BMP-4 (100 ng/ml) or activin A (100 ng/ml) in fresh medium without insulin after overnight starvation. Fifteen minutes after the addition of each growth factor as indicated on the panel. The data are represented as means ± SE (n = 3). *P<0.05. (D) The cells after growth factor starvation were stimulated with FGF-2 (10 ng/ml) and activin A (10 or 100 ng/ml) together with U0126 (5 μM) and GFX (5 μM) or Gö6976 (5 μM) in fresh medium without insulin for 15 minutes. Fifteen minutes after the addition of each growth factor/inhibitor as indicated on the panel. The data are represented as means ± SE (n = 3). *P<0.05.
doi:10.1371/journal.pone.0054122.g002

cantly reduced phosphorylation of not only AKT, but also ERK-1/2 and GSK-3β.

Neither BMP-4 nor activin A in the absence of FGF-2 induced the phosphorylation of AKT, ERK-1/2, or GSK-3β in 201B7 iPS cells (Fig. 2C, Fig. S1C). From our previous report that activin A acts synergistically with FGF-2 in stimulating the phosphorylation of ERK-1/2 [20], we speculated that activin A may increase the phosphorylation of GSK-3β synergistically with FGF-2. Addition

of increasing concentrations of activin A with FGF-2 increased phosphorylation of both GSK-3β and ERK-1/2 in a dose-dependent manner in H9 hES cells (Fig. 2D, Fig. S1D). Addition of U0126 with FGF-2 and activin A had little influence on phosphorylation of both AKT and GSK-3β, and completely inhibited phosphorylation of ERK-1/2. Addition of GFX together with U0126 in the presence of FGF-2 and activin A not significantly increased phosphorylation of AKT, while it completely inhibited phosphorylation of both ERK-1/2 and GSK-3β (Fig. 2D, Fig. S1D). A selective inhibitor of classical PKC (α, β, and γ isoforms) [29], Gö6976 had little influence on phosphorylation of AKT and decreased phosphorylation of GSK-3β less than GFX. These results suggested that FGF-2-induced PKC stimulated phosphorylation of GSK-3β and that GFX inhibited the PKC-induced phosphorylation of GSK-3β, but it increased phosphorylation of AKT (Fig. S2).

Effect of GFX and PMA on colony morphology of the cells

To confirm the speculation that PKCs play roles in regulating self-renewal in hPS cells, the effect of the PKC activator PMA with several kinase inhibitors on the culture of 201B7 hiPS cells was determined (Fig. 3A). Treatment with PMA scattered the iPS cell colony dramatically. PMA-treatment with LY-294002, lithium chloride (LiCl, GSK inhibitor), Y-27632, or U0126 did not reverse the morphological change whereas GFX negated the effect of PMA on cultured 201B7 cells. Gö6976 did not negate the effect of PKC. The effect of Gö6976 was compared with that of GFX on ALP-activity of the cells: GFX with FGF-2 increased the ALP-activity of 201B7 iPS cells, while Gö6976 with FGF-2 had little effect on ALP-activity of the cells (Fig. 3B). GFX increased colony forming efficiency in hESF9 medium (Fig. 3C). Gö6976 did not increase the colony sizes of 201B7 cells and also cell numbers of H9 and 201B7 cells whereas GFX increased the colony sizes and also cell numbers (Fig. 3D, 3E, 3F). PMA activates PKCα, β, γ, δ, ε, η, and θ whereas GFX inhibits PKCα, β, γ, δ, ε, and ζ isoforms. Gö6976 inhibits PKCα, β, and γ isoforms. These results and findings suggested that PKCδ or ε isoforms regulate undifferentiated state of hPS cells.

Isoform-specific function of PKCs in FGF-2 signaling

To determine the isoform-specific function of PKCs on FGF-2 signaling, at first the expression of 11 PKC isoform genes in 201B7 iPS cells was determined by RT-PCR. The results showed that the cells expressed all of 11 PKC isoforms examined here (Fig. 4A). The PKC inhibitor results described above suggested that PKCδ or PKCε might be responsible for GSK-3β phosphorylation but there is a possibility that PKCζ might also be involved. Then, we examined whether FGF-2 stimulated phosphorylation of PKCδ, PKCε or PKCζ with or without GFX. Image analysis of western blotting showed that the phosphorylation of PKCδ and PKCε was increased in a time-dependent manner after stimulation of FGF-2 and the phosphorylation of PKCζ was increased in 15 min after stimulation of FGF-2 and then decreased, suggesting that activation mechanism of PKCζ might be related with GSK-3β phosphorylation (Fig. 4B). GFX diminished the increased phosphorylation of all three PKCs. These result indicated that FGF-2 induced PKCδ, PKCε, and PKCζ in hPS cells.

We next examined the effects of short interfering RNA (siRNA) targeting PKCδ, PKCε or PKCζ on FGF-2 signaling in 201B7 iPS cells. The efficacy and specificity of siRNA was confirmed by quantitative RT-PCR (Fig. S3A). The expression of the targeted PKC genes was inhibited for at least 60%. The phosphorylation levels of AKT, ERK-1/2 and GSK-3β were measured in these PKCs-knockdown cells by AlphaScreen® SureFire® assay kit. The results showed that knockdown of PKCδ, and PKCζ did not affect FGF-2-induced AKT phosphorylation while knockdown of PKCε significantly reduced it (Fig. 4C). Knockdown of either PKCε or PKCζ isoform significantly decreased FGF-2-induced ERK-1/2 phosphorylation. GFX which is reported to target PKCα, β, γ, δ, ε and ζ isoforms did not change the level of FGF-2-induced ERK-1/2 phosphorylation, as shown above (Fig. 2 and Fig. S1). These results implied that cross-interaction among PKC isoforms might affect on the level of FGF-2-induced ERK-1/2 phosphorylation. Then, the cells were treated with the inhibitory peptide cocktail for all isoforms (PKCα, β, γ, δ, ε and ζ), or the inhibitory peptide cocktail for PKCδ, ε, and ζ. The inhibitory peptide cocktail for all isoforms did not affect on FGF-2-induced ERK-1/2 phosphorylation. On the other hand, the inhibitory peptide cocktail for PKCδ, ε, and ζ inhibited the ERK-1/2 phosphorylation (Fig. S4). These results suggested that inhibitions of all isoforms neutralized the reducing effect on FGF-2-induced ERK-1/2 phosphorylation by the inhibition of PKCε and ζ. GSK-3β phosphorylation was significantly reduced by the knockdown of all three PKC isoforms, compared with that by non-target siRNA. These results suggest that FGF-2 induced PKCs, followed by phosphorylation of ERK-1/2 and GSK-3β in hPS cells (Fig. S3B). From these results, we showed that FGF-2 induced PKCδ, ε, and ζ, resulting in stimulation of differentiation in hPS cells which might cause instability of the self-renewal state of hPS cells and that GFX targets these PKC isoforms in hPS cells, resulting in enhanced self-renewal of hPS cells.

Stability of self-renewal of hPS cells in the presence of inhibitors of ERK-1/2 and PKC

Based on the results above, we hypothesized that inhibition of both PKC and ERK-1/2 might provide stable culture of hPS cells in our minimal defined medium hESF9 with activin A. Dissociated single hPS cells were inoculated on FN in hESF9 medium supplemented with activin A (10 ng/ml) [8,20], U0126 (5 μM) or GFX (5 μM). When dissociated single cells were cultured in hESF9, hESF9 + activin A, hESF9 + U0126, or hESF9 + activin A + U0126, many cells died or differentiated (Fig. 5A). On the other hand, when dissociated single cells were cultured in hESF9 + activin A + GFX, or hESF9 + activin A + GFX + U0126 (2i), cells could proliferate enough to be passaged. However, usually after 3 passages, epithelial-like cells appeared in the culture of hESF9 + activin A + GFX condition (Fig. S5A). Immunocytochemical analysis by image analyzer showed that ratio of OCT3/4-positive cell population in the culture of hESF9 + activin A + GFX + U0126 (2i) condition was slightly higher than that in the culture of hESF9 + activin A + GFX (Fig. S5B and S5C). Gene expression in the cells cultured in these culture conditions was analyzed by real-time PCR (Fig. 5B). The expression of an endoderm marker, FOXA2, and a mesoderm marker, T were increased by activin A but it was significantly reduced by the addition of U0126. When the cells were cultured in hESF9 + activin A + U0126 + GFX, both FOXA2 and T were inhibited at lower level and also the undifferentiated makers, NANOG and OCT3/4 were maintained at higher ratio in the cells than those in other culture conditions. Next, the serial culture of dissociated single cells of hES H9, hES KhES4, hiPS 201B7 and hiPS Tic [33] cell lines were tested in hESF9 medium supplemented with activin A (10 ng/ml), U0126 (5 μM) and GFX (5 μM) (designated hESF9a_{2i} medium; Table S1). Dissociated single hPS cells were grown on FN in hESF9a_{2i} medium for 3 passages. Phase-contrast image showed that cell morphology seemed undifferentiated although they did not form hPS typical cell colony. OCT3/4 expression profiles were confirmed by immunofluorescence analysis using image analyzer,

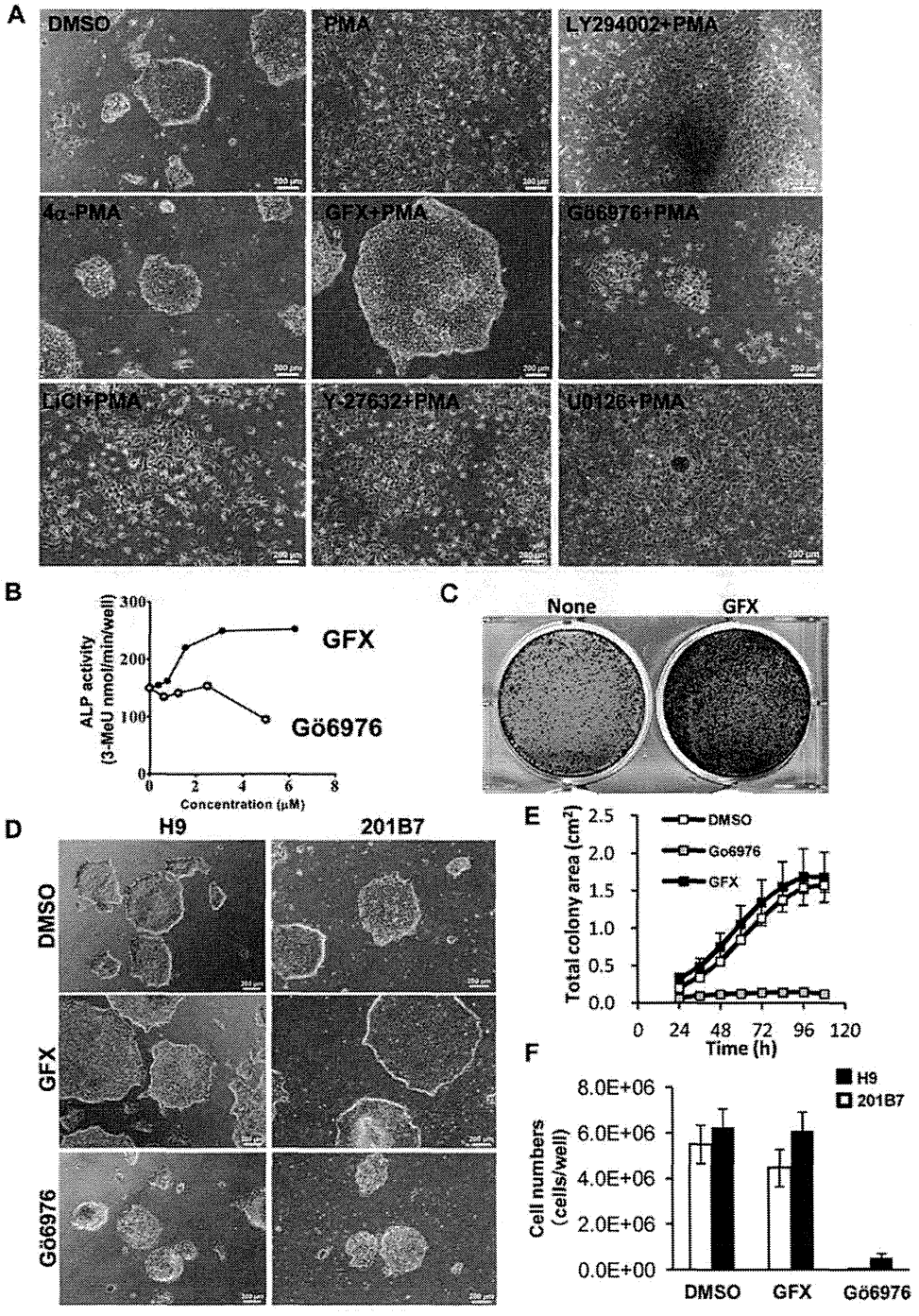

Figure 3. The effect of PKC on the morphologies of hPS cells with or without GFX. (A) Phase-contrast image of 201B7 hiPS cells cultured in feeder-free hESF9 defined medium on FN 24 hours after treatment with DMSO, PMA (10 nM), 4α-PMA (10 nM), GFX (5 μM), PMA (10 nM) with GFX (5 μM), PMA (10 nM) with Gö6976 (5 μM), PMA (10 nM) with LY-294002 (50 μM), PMA (10 nM) with LiCl (1 mM), PMA (10 nM) with Y-27632 (10 μM), or PMA (10 nM) with U0126 (20 μM). An inactive PMA analogue, 4α-PMA is used as negative control. Scale bars, 200 μm. (B) Quantitative ALP-based assay of 201B7 hiPS cells cultured in feeder-free hESF9 medium with GFX (closed circle) or Gö6976 (open circle) as indicated concentrations. (C) Colony forming efficiency of dissociated single hPS cells cultured with or without GFX. Dissociated single 201B7 cells seeded at 250,000 cells/well were grown on a 6-well plate coated with FN (2 μg/cm^2) in hESF9 medium supplemented with and without 1 μM GFX. A in 5 days and stained with ALP fast-red substrate. (D) Phase-contrast image of 201B7 hiPS cells or H9 hES cells cultured in feeder-free hESF9 medium with DMSO (open square), GFX (5 μM, gray square), or Gö6976 (5 μM, closed square). (E) Growth of cell colony area of hPS cells in the presence of GFX or Gö6976. The whole images of 201B7 cell colonies grown in a 6-well-plate coated with FN in the presence of DMSO, GFX or Gö6976 in hESF9 medium was measured by an analysis software, Cell-Quant. The images were captured every 12 hours in live cell imaging system Biostation CT. The data are represented as means ± SD (n = 3). (**F**) Cell growth of hPS cells in the presence of GFX or Gö6976. The numbers of H9 (open bars) and 201B7 cells (closed bars) grown in a 6-well-plate coated with FN in the presence of DMSO, GFX or Gö6976 in hESF9 medium were counted on 5 days. The data are represented as means ± SD (n = 3).

doi:10.1371/journal.pone.0054122.g003

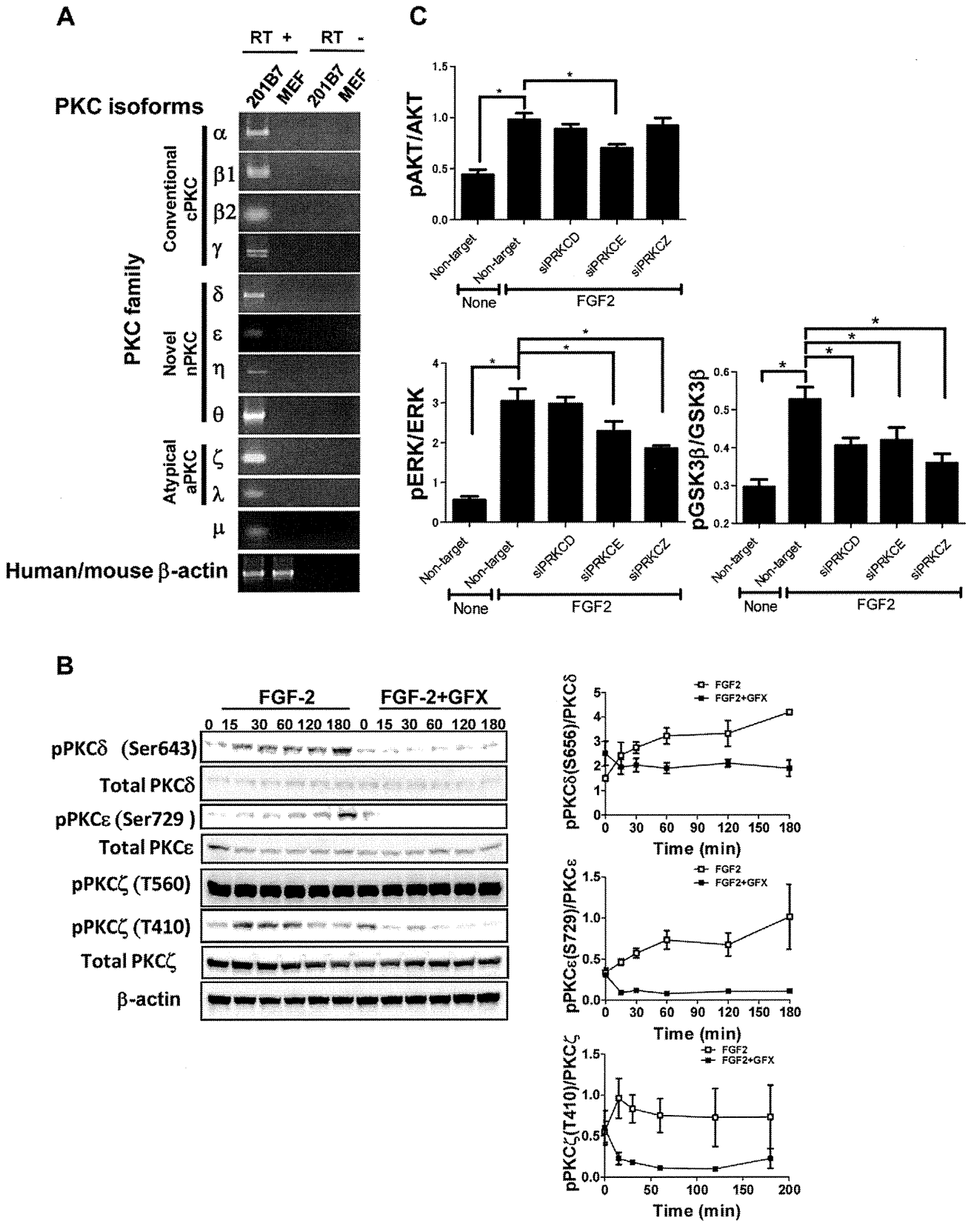

Figure 4. Specific-isoform of PKCs function in FGF-2 signaling. (**A**) RT-PCR analysis of PKC isoform expression. Total RNA was extracted from the undifferentiated 201B7 hiPS cells cultured on feeder cells (CF-1) with KSR-based medium or the feeder cells. Primers were listed in Table S3. (**B**) Phosphorylation of PKCδ, ε, or ζ isoforms induced by FGF-2 (open square) with GFX (closed square). 201B7 hiPS cells were stimulated with FGF-2 (100 ng/ml) after overnight starvation and incubated with or without GFX (5 μM) for 180 minutes. The cells were lysed and followed by western blot

analysis using an antibody detecting the phosphorylation or total protein amount of PKCδ, PKCε, or PKCζ. Protein content quantified from the gel blot images (n = 3). The values of the y-axis are the ratio of each phosphorylation to each total signal protein. (**C**) FGF-2 signaling in hPS cells with specific PKC isoforms-targeting siRNA. 201B7 iPS cells were transfected with specific PKCδ, ε, or ζ isoforms-targeting siRNA or non-targeting siRNA. The phosphorylation levels of the cells treated with FGF-2(100 ng/ml) after overnight starvation were measured by AlphaScreen® SureFire® assay kit. The values of the y-axis are the ratio of each phosphorylation to each total signal protein. The data are represented as means ± SE (n = 3). *P<0.05.
doi:10.1371/journal.pone.0054122.g004

suggesting that the hPS cells maintained undifferentiated state. Another undifferentiated maker, TRA-1-60 expression was also confirmed in hPS cells grown in hESF9a$_{2i}$ medium for 3 passages (Fig. S6).

Serial culture more than 10 passages of undifferentiated H9 hES cells and 201B7 hiPS were tested on FN in hESF9a$_{2i}$ medium. Undifferentiated morphologies of 201B7 hiPS (Fig. S7A) and H9 hES colonies (Fig. S8A) were maintained for more than 30 passages using the conventional passage procedure. The growth rates of H9 hES and 201B7 hiPS cells in hESF9a$_{2i}$ medium were similar to those of cells grown in the conventional KSR-based medium on feeders (Figs. S7B and S8B). The cells retained expression of stage-specific embryonic antigen (SSEA)-4 [34], cell surface antigens TRA-1-60 [35], TRA-1-81 [35], CD90 (Thy-1) [36], and TRA-2-54 [36] (alkaline phosphatase), but did not express SSEA-1 [37] or a neural marker A2B5 [36] (Fig. S7C, S7D and S8C, S8D). The cells retained normal karyotypes (Fig. S9A), pluripotency in vitro (Fig. S9B) and in vivo (Fig. S9C). These results confirmed that inhibition of both ERK-1/2 and PKC supported the self-renewal of hPS cells.

Discussion

Many studies reported that FGF-2 activates both the MAPK/ERK, and PI3K/AKT pathways, which are important for maintaining pluripotency and viability in hPS cells [9,14–16]. However, FGF-2 downstream signaling is not clearly understood in hPS cells. In this study using a minimum essential defined culture system [8,20], we showed that FGF-2 activated PI3K/AKT and MEK/ERK-1/2, but also PKCδ, ε and ζ isoforms in hPS cells (Fig. 6).

The PKC family has been implicated as an intracellular mediator of several neurotransmitters, hormones, tumor promoters, α1-adrenergic agonists, and phorbol esters, and it is important in the regulation of growth, differentiation, cell death, and neurotransmission [38]. The PKC family comprises classical (PKCα, β, and γ; activated by Ca^{2+} and phorbol esters), novel PKC (PKCδ, ε, η, and θ; activated by phorbol esters but not regulated by Ca^{2+}), and atypical PKC (PKCζ and PKCι/λ; not activated by Ca^{2+} or phorbol esters). Different isoforms may perform distinct functions, as suggested by their differential pattern of localization, differences in condition of activation, and some differences in substrate specificity [39–40]. PKC has previously been implicated in GSK-3 regulation [41–42]. Fang et al. [43] showed that PKCα, βII, γ, η, and δ were capable of phosphorylating GSK-3β while PKCε and PKCζ did not phosphorylate GSK-3 by in vitro kinase assays; also, expression of constitutively active PKCα, βI, γ, η enhanced phosphorylation of cotransfected GSK-3β in HEK293 cells. On the other hand, Eng et al. [15] reported that negative construct of PKCε isoform prevented phosphorylation of GSK-3 in migrating fibroblasts._These pieces of evidence suggested that specific isoforms of PKC have different roles in different types of cells. Shuibing et al. [44] reported that activation of PKCα and/or β directs the pancreatic specification of hES cells. Recently, Feng et al. [45] reported that activation of PKCδ induces extraembryonic endoderm differentiation of hES cells. These studies suggested that PKCs might be involved in differentiation of hPS cells. Our study showed that FGF-2 induced PKCδ, ε, and ζ, resulting in phosphorylation of GSK-3β, ERK-1/2, or AKT. Chou, et al. [46] reported that the phosphorylation of PKCζ was regulated by PI3-kinase and PDK-1 in NIH 3T3 fibroblasts. Intriguingly, PKCζ can stimulate GSK-3 activity, by relieving PKB-imposed inhibition [47]. In mouse ES cells, it has been shown that PKCζ plays an important role in inducing lineage commitment in mESCs through a PKCζ–nuclear factor kappa-light-chain-enhancer of activated B cells signaling axis [48]. However, PKC inhibition does not change phosphorylation of ERK-1/2 or GSK-3β. In view of the fact that LIF mainly regulates self-renewal in mouse ES cells, isoform specific function might be cross-regulated by other signaling in the cells. Further, our study showed that the combination effect by inhibition of PKCα, β, γ, δ, ε, and ζ was different from that by inhibition of PKCε and ζ, suggesting that each PKC might interact in different contexts and also PKCδ, ε, and ζ might have different activation mechanisms in hPS cells. It is needed further investigation in future.

GSK-3β is inhibited by phosphorylation stimulated by the canonical Wnt signal pathway, which is followed by the accumulation of β-catenin to the nucleus [49]. From the above findings, it follows that FGF-2 may activate Wnt signaling through PKC leading to differentiation of hPS cells. This conclusion contradicts the findings of previous studies demonstrating that canonical Wnt signaling supports self-renewal of stem cells [50–52]. However, it is consistent with a study showing that canonical Wnt signaling does not appear to promote stem cell maintenance, which prevents differentiation of stem cells [53]. On the other hand, some studies have shown a dual function for Wnt signaling in hES cells in that the pathways of self-renewal or differentiation are dependent on the presence of hES cell supporting factors [51–52]. Recently, Ding et al. [32] showed that FGF-2 modulates Wnt signaling through AKT/GSK-3β signaling and suggested that the differences in the results could be due to the culture platform. Our findings suggest that GSK-3β activity is regulated by FGF-2 through both PI3K/AKT and PKC pathways. AKT/GSK-3β signaling may support self-renewal whereas PKC/GSK-3β may promote cell differentiation of hPS cells. However, GFX decreased the phosphorylation level of GSK-3β to lower level than non-treatment. GSK-3β signaling might be stimulated also by other signal pathway in hPS cells. Target genes of these pathways and further regulation mechanisms in GSK-3β signaling should be analyzed in future.

TGF-β/activin/nodal pathways are thought to crosstalk with FGF signaling in regulating hPS cells. Vallier et al. [1–2,54] demonstrated that activin/nodal pathway in co-operation with FGF-2 is necessary for the maintenance of pluripotency in hES cells. We recently reported that activin A enhances FGF-2-induced ERK-1/2, which permits neural and mesendodermal differentiation of hES cells [20]. In this study we showed that activin A enhanced FGF-2-induced phosphorylation of not only ERK-1/2 but also GSK-3β. Inhibition of these pathways provided stable culture of hPS cells for long-term. In this study, we used both GFX and U0126 to inhibit these pathways. GFX targeting all of PKCα, β, γ, δ, ε, and ζ had no inhibitory effect on ERK-1/2 pathway although siRNA targeting PKCε or PKCζ decreased it. If more specific inhibitor is developed in future, it would be more useful.

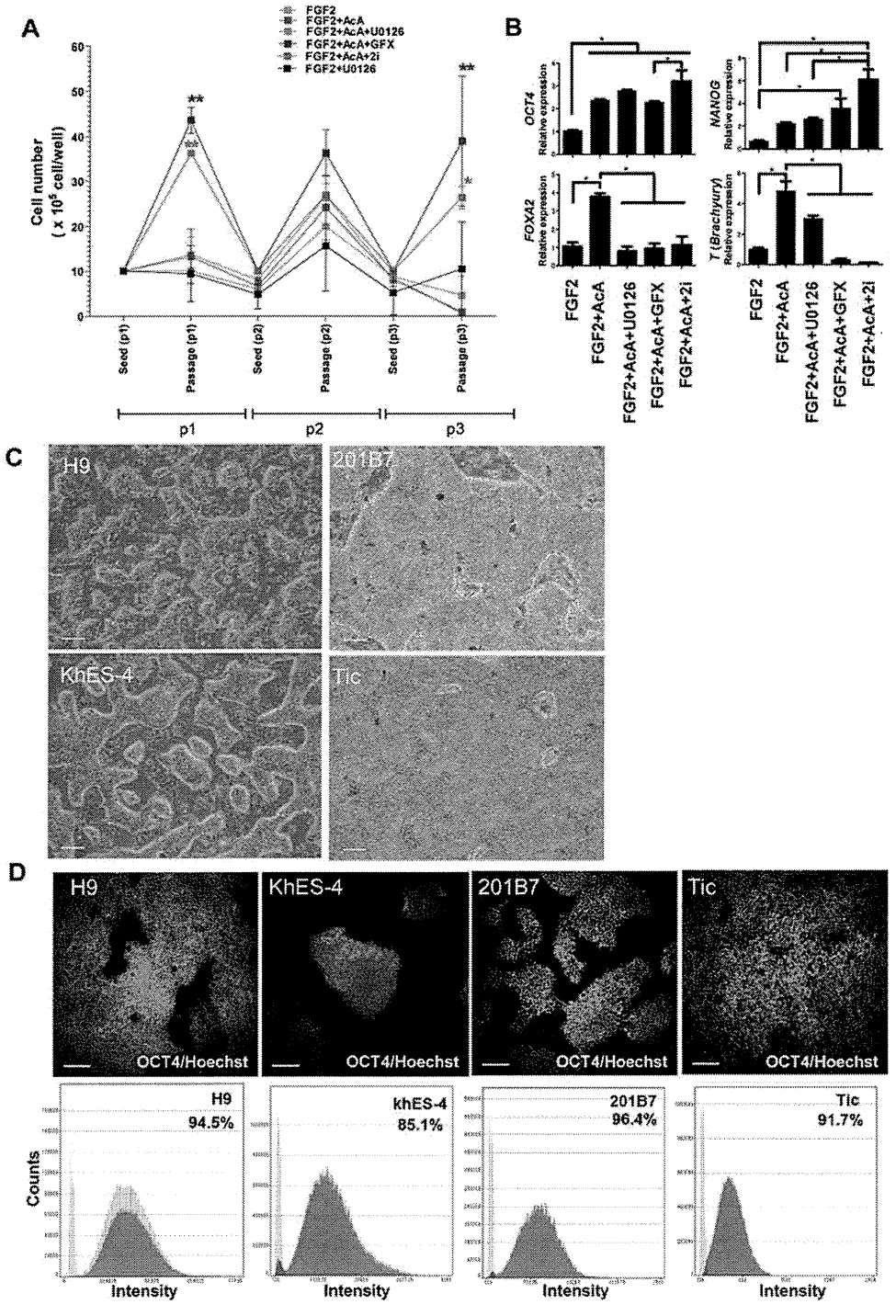

Figure 5. Single cell culture of hPS cells in the hESF9a$_{2i}$ medium. (A) Cell growth of dissociated single H9 hES cells cultured in each indicated condition for three passages. Cells were reseeded at the cell density of 1×10^6 cells/well every 5 days. When the cells were passages, cell numbers were counted. Cell growth in the hESF9a$_{2i}$ medium was significantly different ($P<0.05$) from hESF9 (FGF-2), FGF-2 + activin A, FGF-2 + activin A + U0126. Cell growth in hESF9a + GFX was significantly different ($P<0.05$) from hESF9 (FGF-2), FGF-2 + activin A, FGF-2 + activin A + U0126, and FGF2 + U0126. The data are represented as means ± SE (n = 3). (**B**) Gene expression in the hPS cells cultured in each indicated condition for three passages. The gene expression levels of NANOG, OCT3/4, FOXA2, T in the cells were measured by real-time RT-PCR. On the y axis, the gene expression level in the cells cultured with FGF-2 in a experiment was taken as 1.0. The data are represented as means ± SE (n = 3). *$P<0.05$. (**C**) Phase-contrast image of hPS cells grown on FN in hESF9a$_{2i}$ medium for 3 passages. The cells were dissociated into single cells for passage, and reseeded at a ratio of 1:3 - 1:5 every five days. Scale bars, 200 μm. (**D**) OCT3/4 expression in hPS cells grown on FN in hESF9a$_{2i}$. The cells grown in hESF9a$_{2i}$ as described above in Figure 5C were reseeded on a 6-well-plate and cultured for 5 days. The cells stained with anti-OCT3/4 antibody were visualized with Alexa Fluor 488 (upper panels). Nuclei were stained with Hoechst 33342 (blue). Scale bars, 200 μm. Whole cell images in whole plate were captured and OCT3/4 expression profiles were analyzed by Image Analyzer (lower panels). Antigen histogram (red); control histogram (green); Y axis is cell numbers and X axis is fluorescence intensity for anti-OCT3/4 antibody.

doi:10.1371/journal.pone.0054122.g005

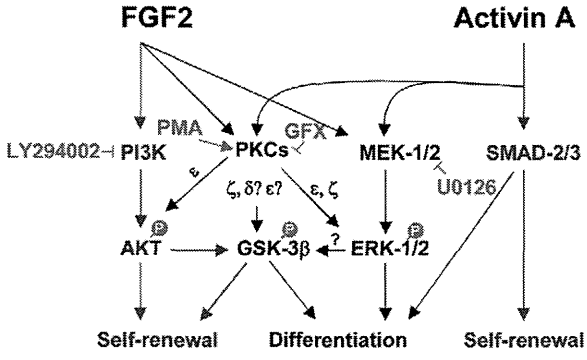

Figure 6. Model for the molecular mechanism of PKCs regulating self-renewal or differentiation in hPS cells. Our study suggested a model that FGF-2 activates PI3K/AKT, MEK/ERK-1/2, and PKCε/δ/ζ. PKCε, δ, and ζ inactivates directly or indirectly GSK-3β by phosphorylation which promotes differentiation of hPS cells. PKCε and ζ activates ERK-1/2 which promotes differentiation of hPS cells. Activin A activates SMAD-2/3 which controls self-renewal and differentiation while activin A together with FGF-2 activates both ERK-1/2 and PKCs. Inhibition of both ERK-1/2 and PKCs pathway provides a metastable undifferentiated state of hPS cells. Blue arrow indicated pathway promoting hPS cell self-renewal and black arrow indicated pathway promoting hPS cell differentiation.
doi:10.1371/journal.pone.0054122.g006

To maintain undifferentiated state, balancing among ERK-1/2, PI3K, SMAD, and PKC signal pathways may be required in any culture conditions. KSR of which components are not disclosed in public is known to have BMP-4-like activity [55]. Some components including BMP-4 in KSR together with secreting factors from mouse feeders might regulate PKC/ERK-1/2 signaling. Using our defined conditions, more molecules including growth factors would be screened to detect their accurate effects on hPS cells.

In conclusion, our study suggested that FGF-2 induced PI3K/AKT and MEK/ERK-1/2, but also PKCs in hPS cells. PI3K/AKT promotes cell self-renewal whereas the MEK/ERK-1/2, PKC/ERK-1/2 and PKC/GSK-3β pathways down-regulate hPS cell self-renewal. This study helps to untangle the cross-talk between molecular mechanisms regulating self-renewal and differentiation of hPS cells.

Materials and Methods

Chemicals

A chemical library of kinase inhibitors (Biomol, Plymouth Meeting, PA, USA), LY-294002 (Cell Signaling Technology, Beverly, MA, USA), BIO (Merck, Darmstadt, Germany), U0126 (Promega, Madison, WI, USA), Y-27632 (Wako Pure Chemical, Osaka, Japan), PMA (Sigma, St. Louis, MO, USA), 4α-PMA (Promega) and Gö6976 (Sigma) were dissolved in dimethyl sulfoxide (DMSO). LiCl (Sigma) and GF109203X hydrochloride (Sigma) were dissolved in water.

PKC inhibitory peptides

Membrane-permeable PKCδ inhibitory peptide δV1-1 (SFNSYELGSL: amino acids 8-17 of PKCδ) or PKCε inhibitory peptide εV1-2 (EAVSLKPT: amino acids 14-21 of PKCε) were designed according to the method of Mochly-Rosen [56–57]. The peptides were custom-synthesized by Sigma (purified to >95% by HPLC). Myristoylated PKCα, β, and γ inhibitory peptide and myristoylated PKCζ inhibitory peptide were purchased from Promega and Calbiochem (Darmstadt, Germany), respectively.

Cell culture

The hES cell lines, H9 [10,31] (WA09, WISC Bank, WiCell Research Institute, Madison, WI, USA) and KhES-4 (provided by Kyoto University, Kyoto, Japan), and hiPS cell lines, 201B7 [26] (provided by Dr. Shinya Yamanaka, Kyoto University) and Tic (JCRB1331, JCRB Cell Bank, Osaka, Japan) [33,58] were routinely maintained on mitomycin C-inactivated mouse embryo fibroblast feeder cells (MEF, Millipore Co., Billerica, MA, USA) in an KSR-based medium supplemented with 5 ng/ml (H9, khES-4), 4 ng/ml (201B7) or 10 ng/ml (Tic) human recombinant FGF-2 (Katayama Kagaku Kogyo LTD., Osaka, Japan) previously described [10]. Human ES cells were used following the Guidelines for utilization of human embryonic stem cells of the Ministry of Education, Culture, Sports, Science and Technology of Japan after approval by the institutional ethical review board at National Institute of Biomedical Innovation. The cells were passaged with 1 mg/ml dispase (Roche, Mannheim, Germany) in DMEM/F12 medium and a plastic scraper (Sumitomo Bakelite Co., LTD Tokyo, Japan). The cells were split at a ratio of 1:5–1:8 every 5 days.

Human ES/iPS cell culture in feeder-free and growth factor defined serum-free medium

Prior to culture in feeder-free conditions, the medium was changed from the KSR-based medium to a growth factor-defined serum-free hESF9 medium [8] (Table S1). Two days after the medium change, the cells were harvested with 1 mg/ml dispase or TrypLE (Invitrogen), and reseeded on plastic plates coated with bovine FN (Sigma, 2 μg/cm^2) [21]. For long-term culture, hPS cells were maintained on FN in hESF9 medium supplemented with 10 ng/ml human recombinant activin A (R&D Systems Minneapolis, MN, USA) in the presence of both 5 μM U0126 [20], and 5 μM GFX, designated hESF9a$_{2i}$ medium. The medium was changed every day.

Single hPS cell culturing with two inhibitors

hPS cells were dissociated with TrypLE (Invitrogen) into single cells, and seeded on a 6-well plate coated with FN at the cell density of 1×10^6 cells/well in hESF9, or supplemented with 10 ng/ml activin A, 5 μM U0126, or 5 μM GFX. The medium was changed every day.

Quantitative ALP activity-based high-throughput screening assay

The hPS cells were dissociated with accutase into single cells and seeded at 5×10^4 cells/well on a 96-well plate coated with FN (FN, 2 μg/cm^2) in hESF9 medium. Each compound in the chemical library was added at 2.5 μM to each well. After further 5 days-culture, the cells were washed with 3-[4-(2-Hydroxyethyl)-1-piperazinyl] propanesulfonic acid (EPPA) buffer (30 mM, pH 8.2). Fluorescence ALP substrate (0.2 mM, 4-methylumbelliferyl phosphate) [59] in EPPS buffer was added into the wells. After incubation for 30 min at 37°C, EPPS buffer (100 mM, pH 7.7) supplemented with 1 M K_2HPO_4 was add to terminate the enzyme reaction. The amount of 4-methylumbelliferone (4-MeU) produced via the enzyme reaction was measured with a fluorescence microplate reader (Gemini EM, Molecular Devices, Menlo Park, CA). The specific activity of ALP was quantified by reference to a standard fluorescence curve generated with known concentrations of 4-MeU (Sigma).

Colony formation assay

Dissociated single hPS cells were seeded at 10,000–250,000 cells/well on a 6-well plate coated with FN (2 μg/cm^2) in hESF9 medium supplemented with and without 1 μM GFX. After 5-days-culture, the colonies were fixed in 4.5 mM citric acid, 2.25 mM sodium citrate, 3.0 mM sodium chloride, 65% methanol, and 3% formaldehyde for 5 min, and stained with ALP fast-red substrate (Sigma) for 15 min at room temperature.

Immunocytochemistry

Immunocytochemistry was performed as described previously [20,60]. The image analysis was performed with In Cell analyzer 2000 and Developer tool box software (GE Healthcare, Little Chalfont, Buckinghamshire, UK), or a confocal microscope (Carl Zeiss). The primary and secondary antibodies used were listed in Table S2.

Western blotting

Western blots were performed as described previously [8,20,60]. Protein (2 μg/lane) was separated by 12.5% SDS-PAGE and transferred to polyvinylidene fluoride (PVDF) membranes (Millipore). The membranes were reacted with primary antibodies, peroxidase-conjugated secondary antibodies, and ECL Plus reagent (GE Healthcare). Protein bands were visualized using LAS-4000 imager (Fujifilm, Tokyo, Japan). The primary antibodies used were listed in Table S2.

AlphaScreen assay

AlphaScreen® SureFire® Cell-based Assay (Perkin-Elmer, Waltham, MA, USA) was performed to measure phosphorylation of AKT-1/2/3, ERK-1/2, and GSK-3β in the cells according to the manufacturer's instructions. Materials used were listed in Table S2. The fluorescence signal was measured using an EnSpire™ plate reader (PerkinElmer).

Gene expression analysis

Total RNA extracted from cultured cells using RNeasy Mini kit (Qiagen, Valencia, CA, USA) were treated with DNase I to remove any genomic contamination, and reverse-transcribed using Superscript VILO cDNA synthesis kit (Invitrogen) according to the manufacturer's instructions. For RT-PCR, PCR products were amplified with AmpliTaq Gold DNA polymerase (Applied Biosystems, Foster City, CA, USA), following manufacturer's instruction. The DNA was separated by gel electrophoresis and visualized under ultraviolet light for photography. For quantitative real-time RT-PCR, PCR was performed based on the TaqMan or the SYBR Green gene expression technology in a 7300 Real Time PCR System (Applied Biosystems), following manufacturer's instruction. Threshold cycles were normalized to the housekeeping gene GAPDH and translated to relative values. Specific primers used are listed in Tables S3 and S4. For PCR-array, TaqMan low-density human stem cell pluripotency card PCR array (Applied Biosystems, Foster City, CA) was performed as previously described [61]. Expression levels were all normalized against the housekeeping gene β-actin. The relative expression levels of each gene in embryoid bodies were compared to the levels in H9 hES cells or 201B7 hiPS cells grown on feeders in KSR-based medium.

Transfections with siRNA

Transfections with siRNA were performed using Dharmafect1 (Dharmacon, Chicago, USA) as previously described [62]. Prior to transfection, the hiPS cells were incubated with ROCK inhibitor Y-27632 (10 μM) for 1 hour and dissociated with TrypLE (Invitrogen) and pelleted by centrifugation. To prepare siRNA/lipid solutions, 50 pmol of siRNAs were diluted in 100 μl of hESF9 medium. In a separate tube, 6 μl of Dharmafect1 was diluted in 100 μl of hESF9 medium. The solution of the two tubes were mixed and incubated at room temperature for 20 mins. The resulting 200 μl of siRNA/lipid solution in hESF9 medium was used to resuspend the cell pelleted containing from 1×10^4 to 1×10^5 cells, and suspension incubated at room temperature for 10 min. After incubation, 1.5 ml of prewarmed hESF9 medium containing ROCK inhibitor (10 μM) was added and the suspension transferred into a FN-coated well of 24-well or 6-well plate, followed by culture for 24 hour. After recovery in fresh hESF9 medium, cells were transfected again at 24 hours. Total RNAs or proteins were extracted for analysis 72 hours after the fast transfection. siRNAs were listed as Table S4.

Live cell imaging analysis

After seeded on a 6-well plate coated with FN, the cells were incubated in a live cell imaging system, BioStation CT (Nikon Instruments Inc., Tokyo, Japan) at 37°C 10% CO_2. The images were captured every 12 hours and analyzed by a soft ware CL-Quant (Nikon Instruments Inc.).

Cell Growth

The cells were inoculated on a 6-well plate coated with FN at the cell density of 250,000 cells/well in hESF9 medium including 10 ng/ml FGF-2, supplemented with 0.1% DMSO, GFX in H_2O, or Gö6976 in DMSO. After 5 days culture, the cell numbers were counted by Coulter Counter (Beckman Coulter, Inc).

Flow cytometry

Flow cytometry was performed as described previously [61] with a FACS Canto flow cytometer (BD Biosciences). The primary antibodies used were listed in Table S2.

In vitro cell differentiation

In vitro differentiation was induced by the formation of embryoid bodies as described previously [61]. Floating embryoid bodies were maintained in DMEM with 10% FCS for more 14 days.

Teratoma formation

The cells were harvested by dispase treatment, collected into tubes, and centrifuged, and the pellets were suspended in DMEM supplemented ROCK inhibitor. The cells from a confluent one-well in 6-well plate were injected to the rear leg muscle or thigh muscle of a SCID (C.B-17/Icr-scid/scidJcl) mouse (CLEA japan, Tokyo, Japan). Nine weeks after injection, tumors were dissected, weighted, and fixed with 10% formaldehyde Neutral Buffer Solution (Nacalai tesque, Kyoto, Japan). Paraffin-embedded tissue was sliced and stained with hematoxylin and eosin. All animal experiments were conducted in accordance with the guidelines for animal experiments of the National Institute of Biomedical Innovation, Osaka, Japan.

Karyotype analysis

Log phase hPS cells (day 3–4 after subculture) were treated with metaphase arresting solution (Genial Genetic Solutions Ltd., Cheshire, UK) for 5 hr. The treated hPS cells were collected with 0.1% EDTA and processed according to the quality control protocol in the JCRB Cell Bank (http://cellbank.nibio.go.jp/cellbank.html). Chromosome numbers were counted in 20

metaphases, and G-banding karyotype analysis was performed on 20 metaphase cells per sample.

Supporting Information

Figure S1 The phosphorylation of AKT, GSK-3β, and ERK-1/2 was confirmed by western blot analysis using an antibody to AKT, GSK-3β, and ERK-1/2 and their phosphorylated forms. Each gel image is a representative of independent three to five experiments. (**A**) Time course of phosphorylation level of AKT, GSK-3β, and ERK-1/2. H9 hES cells were stimulated with FGF-2 (100 ng/ml) with or without GFX (5 μM) for 180 minutes after overnight starvation of FGF-2 and insulin. (**B**) Effect of inhibitors on phosphorylation level of AKT, GSK-3β, and ERK-1/2. After starvation of FGF-2 and insulin overnight, 201B7 hiPS cells were stimulated with FGF-2 (100 ng/ml) for 15 min with LY294002, GFX, U0126, or BIO or without GFX (5 μM). (**C**) Effect of BMP-4 or activin A on phosphorylation level of AKT, GSK-3β, and ERK-1/2. After starvation of FGF-2 and insulin overnight, 201B7 hiPS cells were stimulated with with FGF-2 (100 ng/ml), BMP-4 (10 ng/ml) or activin A (100 ng/ml). (**D**) Effect of addition of activin A with and without inhibitors on phosphorylation level of AKT, GSK-3β, and ERK-1/2. After starvation of FGF-2 and insulin overnight, H9 hES cells were stimulated with FGF-2 (10 ng/ml) and activin A (10 or 100 ng/ml) together with U0126 (5 μM) and GFX (5 μM) or Gö6976 (5 μM) for 15 minutes. (**E**) Effect of GFX concentration on phosphorylation level of AKT, GSK-3β, and ERK-1/2. After starvation of FGF-2 and insulin overnight, H9 hES cells were stimulated with FGF-2 (100 ng/ml) with GFX at 1~10 μM. The phosphorylation levels in the cells were measured by AlphaScreen® SureFire® assay kit. The values of the y-axis are the ratio of each phosphorylation to each total signal protein. The data are represented as means ± SD (n = 3). *P<0.05.
(TIF)

Figure S2 Summary of the result of the effect of PI3K, MEK-1/2, or PKCs inhibitor on FGF-2-induced phosphorylation of AKT, GSK-3β, and ERK-1/2.
(TIF)

Figure S3 Knockdown efficacy and effect of siRNA targeting PKCδ, ε, and ζ. (**A**) Total RNAs were extracted for analysis 72 hours after the fast transfected to 201B7 iPS cells. The efficacy of siRNA was evaluated by quantitative RT-PCR. siRNAs and primers were listed as Table S4. (**B**) Summary of the result of the PKCδ-, PKCε-, PKCζ-knockdown effect on phosphorylation of GSK-3β and AKT in FGF-2 signaling.
(TIF)

Figure S4 Effect of inhibitory peptides for PKCs on phosphorylation level of ERK-1/2. After starvation of FGF-2 and insulin, the H9 hES cells (right panel) or the 201B7 iPS cells (left panel) were stimulated with FGF-2 (100 ng/ml) for 15 mins with indicated combination of membrane-permeable specific inhibitory peptides for PKC isoforms; PKCα, β, and γ inhibitory peptide (50 μM), PKCδ inhibitory peptide (50 μM), PKCε inhibitory peptide (50 μM), or PKCζ inhibitory peptide (20 μM). The phosphorylation levels in the cells were measured by AlphaScreen® SureFire® assay kit. The values of the y-axis are the ratio of each phosphorylation to each total signal protein. The data are represented as means ± SD (n = 3). *P<0.05.
(TIF)

Figure S5 Culture of hiPS cells in the hESF9 + activin A + 2i or the hESF9 + activin A + GFX conditions. (**A**) Phase-contrast image of H9 hES cells serially cultured in hESF9 + activin A + 2i (hESF9a_{2i}) or hESF9 + activin A + GFX mediums at three passages, as described in Figure 5A and 5B. Scale bars, 200 μm. (**B**) Immunocytochemical staining for OCT3/4 expression of H9 cells cultured as described (A). The H9 hES cells stained with anti-OCT3/4 antibody were visualized with Alexa Fluor 488 (green). Nuclei were stained with Hoechst 33342 (blue). Scale bars, 50 μm. (**C**) Anti-OCT3/4 staining intensity profiles in the cell population grown in the hESF9 + activin A + 2i or the hESF9 + activin A + GFX conditions were analyzed by IN Cell image analyzer (lower panels). Antigen histogram (red); control histogram (green); Y axis is cell numbers and X axis is fluorescence intensity for anti-OCT3/4 antibody.
(TIF)

Figure S6 Immunocytochemical staining of H9, KhES-4, 201B7, and Tic hPS cells for TRA-1-60. The cells grown on FN in hESF9a_{2i} as described in Figure 5C were stained with TRA-1-60 antibody and Alexa Fluor 647-conjugated secondary antibody. Nuclei were stained with Hoechst 33342 (blue). Scale bars, 200 μm.
(TIF)

Figure S7 Long-term culture of hiPS cells in the hESF9a_{2i} medium. Human iPS 201B7 cells were cultured on FN in hESF9a_{2i} medium serially for more than 30 passages. The cells were split at a ratio of 1:3–1:5 every five days. (**A**) Phase-contrast image of 201B7 hiPS cells cultured on FN in hESF9a_{2i} medium. (**B**) A comparison of the growth of 201B7 cells in hESF9a_{2i} medium or KSR-based media. The cells were seeded on feeders in KSR-based medium (closed circles) or on FN in hESF9a_{2i} medium (open circles; mean + s.d. of three experiments. Cell numbers were counted every 2 days. (**C**) Immunocytochemical staining for SSEA-1, SSEA-4, TRA-1-60 and TRA-1-81 (red) expression of 201B7 cells (passage 10) cultured on FN in hESF9a_{2i}. Nuclei were stained with Hoechst 33342 (blue). Scale bars, 200 μm. (**D**) FACS profiles for SSEA-1, SSEA-4, TRA-1-60, TRA-1-81, TRA-2-54, A2B5, CD90, and HLA-Class1 expression of hiPS 201B7 cells (passage 22) cultured on FN in hESF9a_{2i} medium. Antigen histogram (red); control histogram (green); the horizontal bar indicates the gating used to score the percentage of antigen-positive cells.
(TIF)

Figure S8 Long-term culture of hES cells in the hESF9a_{2i} medium. Human ES H9 cells were cultured on FN in hESF9a_{2i} medium serially for more than 30 passages. The cells were split at a ratio of 1:3–1:5 every five days. (**A**) Phase-contrast image of H9 hES cells cultured on FN in hESF9a_{2i} medium. (**B**) A comparison of the growth of H9 hES cells (passage 13, 16, and 17) in hESF9a_{2i} (open circles) or KSR-based media (closed circles). Mean + s.d. of three experiments. (**C**) Immunocytochemical staining for SSEA-1, SSEA-4, TRA-1-60, TRA-1-81, TRA-2-54, A2B5, CD90, and HLA-Class1 expression (red) in H9 hES cells (passage 13). Nuclei were stained with Hoechst 33342 (blue). (**D**) FACS profiles of H9 hES cells (passage 14). Antigen histogram (red); control histogram (green). Scale bars = 200 μm.
(TIF)

Figure S9 Karyotype analysis and differentiation potential of H9 hES cells and 201B7 hiPS cells maintained in hESF9a_{2i} conditions. (**A**) Karyotype analysis of H9 hES cells at passage 15 and 201B7 hiPS cells at passage 21, showing a normal diploid 46, xx karyotype. (**B**) Heat-map of gene expression in H9 hES cells (at passage 10–13) and 201B7 hiPS cells (at passage 10–20) those during in vitro differentiation in triplicate experiments (Sample No. 3–5). TaqMan low density PCR arrays

(Applied BioSystems) were performed as previously described [61]. Expression levels were all normalized against β-ACTIN. The relative level of each gene expression were generated from the undifferentiated H9 hES cell or 201B7 hiPS cells cultured on mitomycin-inactivated mouse embryonic fibroblasts (MEF) in KSR-based medium (Sample No. 1–2). Heat-map colors (red for up-regulation, blue for down-regulation) depict gene expression. (**C**) Teratomas derived from H9 hES cells at passage 44 or 201B7 iPS cells at passage 26 maintained in $hESF9a_{2i}$ conditions.
(TIF)

Table S1 The composition of media used for serum-free culture. * The composition of the basal medium, ESF for culturing mouse ES cells, is described in Furue et al., 2005 [22]. ** hESF9 medium is described in Furue et al., 2008 [8]. *** hESF9a medium is described in Hayashi and Furue et al., 2010 [23].
(DOC)

Table S2 A list of the used antibodies.
(DOC)

Table S3 A list of the used primers for RT-PCR.
(DOC)

Table S4 A list of the used primers for qRT-PCR and siRNAs.
(DOC)

Acknowledgments

We thank Prof. Peter W. Andrews (University of Sheffield, Sheffield, UK) for the valuable comments on the manuscript and generous gift of anti-SSEA-4, A2B5, and Tra-2-54 antibodies, Dr. Jie Na (Tsinghua University, Beijing, China) for the valuable comments and discussions on the manuscript, Dr. Ivana Barbaric (University of Sheffield) for the valuable comments on the manuscript, Dr. Takeshi Tomonaga (National Institute of Biomedical Innovation) for the technical advices, and Dr. Hiroshi Takemori (National Institute of Biomedical Innovation) for the generous gift of the chemical library. We also thank Ayaka Fujiki, Mari Wakabayashi, Naoko Ueda, Akiko Hamada, Yujung Liu, Hiroko Ochi, Eiko Kawaguchi, Midori Hayashida, Yutaka Ozawa, Azusa Ohtani, and Setsuko Shioda for excellent technical support and Dr. J. Denry Sato for editorial assistance.

Author Contributions

Conceived and designed the experiments: MK MKF. Performed the experiments: MK SK DT MS HM SM NH MH KUY AK KY. Analyzed the data: MK. Wrote the paper: MK MKF.

References

1. Vallier L, Reynolds D, Pedersen RA (2004) Nodal inhibits differentiation of human embryonic stem cells along the neuroectodermal default pathway. Dev. Biol. 275: 403–421.
2. Vallier L, Alexander M, Pedersen RA (2005) Activin/Nodal and FGF pathways cooperate to maintain pluripotency of human embryonic stem cells. J Cell Science 118: 4495–4509.
3. James D, Levine AJ, Besser D, Hemmati-Brivanlou A (2005) TGFβ/activin/nodal signaling is necessary for the maintenance of pluripotency in human embryonic stem cells. Development 132: 1273–1282.
4. Pebay A, Wong RC, Pitson SM, Wolvetang EJ, Peh GS, et al. (2005) Essential roles of sphingosine-1-phosphate and platelet-derived growth factor in the maintenance of human embryonic stem cells. Stem Cells 23: 1541–1548.
5. Bendall SC, Stewart MH, Menendez P, George D, Vijayaragavan K, et al. (2007) IGF and FGF cooperatively establish the regulatory stem cell niche of pluripotent human cells in vitro. Nature 448: 1015–1021.
6. Dvorak P, Dvorakova D, Koskova S, Vodinska M, Najvirtova M, et al. (2005) Expression and potential role of fibroblast growth factor 2 and its receptors in human embryonic stem cells. Stem Cells 23: 1200–1211.
7. Avery S, Inniss K, Moore H (2006) The regulation of self-renewal in human embryonic stem cells. Stem Cells Dev. 15: 729–740.
8. Furue MK, Na J, Jackson JP, Okamoto T, Jones M, et al. (2008) Heparin promotes the growth of human embryonic stem cells in a defined serum-free medium. PNAS 105: 13409–13414.
9. Ding VM, Boersema PJ, Foong LY, Preisinger C, Koh G, et al. (2011) Tyrosine phosphorylation profiling in FGF-2 stimulated human embryonic stem cells. PLoS One 6: e17538.
10. Amit M, Carpenter MK, Inokuma MS, Chiu CP, Harris CP, et al. (2000) Clonally derived human embryonic stem cell lines maintain pluripotency and proliferative potential for prolonged periods of culture. Developmental Biology 227: 271–278.
11. Hoffman LM, Carpenter MK (2005) Characterization and culture of human embryonic stem cells. Nat. Biotechnol. 23: 699–708.
12. Xu RH, Peck RM, Li DS, Feng X, Ludwig T, et al. (2005) Basic FGF and suppression of BMP signaling sustain undifferentiated proliferation of human ES cells. Nat. Methods 2: 185–190.
13. Schlessinger J (2004) Common and distinct elements in cellular signaling via EGF and FGF receptors. Science 306: 1506–1507.
14. Dreesen O, Brivanlou AH (2007) Signaling pathways in cancer and embryonic stem cells. Stem Cell Rev. 3: 7–17.
15. Armstrong L, Hughes O, Yung S, Hyslop L, Stewart R, et al. (2006) The role of PI3K/AKT, MAPK/ERK and NFκβ signalling in the maintenance of human embryonic stem cell pluripotency and viability highlighted by transcriptional profiling and functional analysis. Hum. Mol. Genet. 15: 1894–1913.
16. Eiselleova L, Matulka K, Kriz V, Kunova M, Schmidtova Z, et al. (2009) A complex role for FGF-2 in self-renewal, survival, and adhesion of human embryonic stem cells. Stem Cells 27: 1847–1857.
17. Ding VM, Ling L, Natarajan S, Yap MG, Cool SM, et al. (2010) FGF-2 modulates Wnt signaling in undifferentiated hESC and iPS cells through activated PI3-K/GSK3β signaling. J. Cell Physiol. 225: 417–428.
18. Na J, Furue MK, Andrews PW (2010) Inhibition of ERK1/2 prevents neural and mesendodermal differentiation and promotes human embryonic stem cell self-renewal. Stem Cell Research 5: 157–169.
19. Nakanishi M, Kurisaki A, Hayashi Y, Warashina M, Ishiura S, et al. (2009) Directed induction of anterior and posterior primitive streak by Wnt from embryonic stem cells cultured in a chemically defined serum-free medium. FASEB Journal 23: 114–122.
20. Aihara Y, Hayashi Y, Hirata M, Ariki N, Shibata S, et al. (2010) Induction of neural crest cells from mouse embryonic stem cells in a serum-free monolayer culture. International Journal of Developmental Biology 54: 1287–1294.
21. Kusuda Furue M, Tateyama D, Kinehara M, Na J, Okamoto T, et al. (2010) Advantages and difficulties in culturing human pluripotent stem cells in growth factor-defined serum-free medium. In Vitro Cellular and Developmental Biology Animal 46: 573–576.
22. Furue M, Okamoto T, Hayashi Y, Okochi H, Fujimoto M, et al. (2005) Leukemia inhibitory factor as an anti-apoptotic mitogen for pluripotent mouse embryonic stem cells in a serum-free medium without feeder cells. In Vitro Cellular and Developmental Biology Animal 41: 19–28.
23. Hayashi Y, Chan T, Warashina M, Fukuda M, Ariizumi T, et al. (2010) Reduction of N-glycolylneuraminic acid in human induced pluripotent stem cells generated or cultured under feeder- and serum-free defined conditions. PLoS One 5: e14099.
24. Watanabe K, Ueno M, Kamiya D, Nishiyama A, Matsumura M, et al. (2007) A ROCK inhibitor permits survival of dissociated human embryonic stem cells. Nat. Biotechnol. 25: 681–686.
25. Wang X, Lin G, Martins-Taylor K, Zeng H, Xu RH (2009) Inhibition of caspase-mediated anoikis is critical for basic fibroblast growth factor-sustained culture of human pluripotent stem cells. J Biol. Chem. 284: 34054–34064.
26. Takahashi K, Tanabe K, Ohnuki M, Narita M, Ichisaka T, et al. (2007) Induction of pluripotent stem cells from adult human fibroblasts by defined factors. Cell 131: 861–872.
27. Lyssiotis CA, Foreman RK, Staerk J, Garcia M, Mathur D, et al. (2009) Reprogramming of murine fibroblasts to induced pluripotent stem cells with chemical complementation of Klf4. PNAS 106: 8912–8917.
28. Barbaric I, Gokhale PJ, Jones M, Glen A, Baker D, et al. (2010) Novel regulators of stem cell fates identified by a multivariate phenotype screen of small compounds on human embryonic stem cell colonies. Stem Cell Research 5: 104–119.
29. Martiny-Baron G, Kazanietz MG, Mischak H, Blumberg PM, Kochs G, et al. (1993) Selective inhibition of protein kinase C isozymes by the indolocarbazole Gö 6976. J Biol. Chem. 268: 9194–9197.
30. Damoiseaux R, Sherman SP, Alva JA, Peterson C, Pyle AD (2009) Integrated chemical genomics reveals modifiers of survival in human embryonic stem cells. Stem Cells 27: 533–542.
31. Thomson JA, Itskovitz-Eldor J, Shapiro SS, Waknitz MA, Swiergiel JJ, et al. (1998) Embryonic stem cell lines derived from human blastocysts. Science 282: 1145–1147.
32. Boersema PJ, Foong LY, Ding VM, Lemeer S, van Breukelen B, et al. (2010) In-depth qualitative and quantitative profiling of tyrosine phosphorylation using a combination of phosphopeptide immunoaffinity purification and stable isotope dimethyl labeling. Mol. Cell Proteomics 9: 84–99.

33. Nishino K, Toyoda M, Yamazaki-Inoue M, Fukawatase Y, Chikazawa E, et al. (2011) DNA methylation dynamics in human induced pluripotent stem cells over time. PLoS Genet 7: e1002085.
34. Kannagi R, Cochran NA, Ishigami F, Hakomori S, Andrews PW, et al. (1983) Stage-specific embryonic antigens (SSEA-3 and -4) are epitopes of a unique globo-series ganglioside isolated from human teratocarcinoma cells. EMBO Journal 2: 2355–2361.
35. Andrews PW, Banting G, Damjanov I, Arnaud D, Avner P (1984) Three monoclonal antibodies defining distinct differentiation antigens associated with different high molecular weight polypeptides on the surface of human embryonal carcinoma cells. Hybridoma 3: 347–361.
36. Draper JS, Pigott C, Thomson JA, Andrews PW (2002) Surface antigens of human embryonic stem cells: changes upon differentiation in culture. Journal of Anatomy 200: 249–258.
37. Solter D, Knowles BB (1978) Monoclonal antibody defining a stage-specific mouse embryonic antigen (SSEA-1). PNAS 75: 5565–5569.
38. Nishizuka Y (1995) Protein kinase C and lipid signaling for sustained cellular responses. FASEB J. 9: 484–496.
39. Newton AC (1997) Regulation of protein kinase C. Curr. Opin. Cell Biol. 9: 161–167.
40. Mochly-Rosen D, Gordon AS (1998) Anchoring proteins for protein kinase C: a means for isozyme selectivity. FASEB J. 12: 35–42.
41. Goode N, Hughes K, Woodgett JR, Parker PJ (1992) Differential regulation of glycogen synthase kinase-3β by protein kinase C isotypes. J Biol. Chem. 267: 16878–16882.
42. Kaidanovich-Beilin O, Woodgett JR (2011) GSK-3: Functional Insights from Cell Biology and Animal Models. Front. Mol. Neurosci. 4: 40.
43. Fang X, Yu S, Tanyi JL, Lu Y, Woodgett JR, et al. (2002) Convergence of multiple signaling cascades at glycogen synthase kinase 3: Edg receptor-mediated phosphorylation and inactivation by lysophosphatidic acid through a protein kinase C-dependent intracellular pathway. Mol. Cell. Biol. 22: 2099–2110.
44. Chen S, Borowiak M, Fox JL, Maehr R, Osafune K, et al. (2009) A small molecule that directs differentiation of human ESCs into the pancreatic lineage. Nat. Chem Biol. 5: 258–265.
45. Feng X, Zhang J, Smuga-Otto K, Tian S, Yu J, et al. (2012) Protein Kinase C Mediated Extraembryonic Endoderm Differentiation of Human Embryonic Stem Cells. Stem Cells 30:461–470.
46. Chou MM, Hou W, Johnson J, Graham LK, Lee MH, et al. (1998) Regulation of protein kinase C ζ by PI 3-kinase and PDK-1. Curr. Biol. 8: 1069–1077.
47. Doornbos RP, Theelen M, van der Hoeven PC, van Blitterswijk WJ, Verkleij AJ, et al. (1999) Protein kinase Cζ is a negative regulator of protein kinase B activity. J Biol. Chem. 26: 8589–8596.
48. Dutta D, Ray S, Home P, Larson M, Wolfe MW, et al. (2011) Self-Renewal Versus Lineage Commitment of Embryonic Stem Cells:Protein Kinase C Signaling Shifts the Balance. Stem Cells 29: 618–628.
49. Moon RT, Kohn AD, De Ferrari GV, Kaykas A (2004) WNT and β-catenin signalling: diseases and therapies. Nat. Rev. Genet. 5: 691–701.
50. Sato N, Meijer L, Skaltsounis L, Greengard P, Brivanlou AH (2004) Maintenance of pluripotency in human and mouse embryonic stem cells through activation of Wnt signaling by a pharmacological GSK-3-specific inhibitor. Nat. Medicine 10: 55–63.
51. Dravid G, Ye Z, Hammond H, Chen G, Pyle A, et al. (2005) Defining the role of Wnt/β-catenin signaling in the survival, proliferation, and self-renewal of human embryonic stem cells. Stem Cells 23: 1489–1501.
52. Cai L, Ye Z, Zhou BY, Mali P, Zhou C, et al. (2007) Promoting human embryonic stem cell renewal or differentiation by modulating Wnt signal and culture conditions. Cell Research 17: 62–72.
53. Sumi T, Tsuneyoshi N, Nakatsuji N, Suemori H (2008) Defining early lineage specification of human embryonic stem cells by the orchestrated balance of canonical Wnt/β-catenin, Activin/Nodal and BMP signaling. Development 135: 2969–2979.
54. Vallier L, Mendjan S, Brown S, Chng Z, Teo A, et al. (2009) Activin/Nodal signalling maintains pluripotency by controlling Nanog expression. Development 136: 1339–1349.
55. Ying QL, Nichols J, Chambers I, Smith A (2003) BMP induction of Id proteins suppresses differentiation and sustains embryonic stem cell self-renewal in collaboration with STAT3. Cell 115: 281–292.
56. Chen L, Hahn H, Wu G, Chen CH, Liron T, et al. (2001) Opposing cardioprotective actions and parallel hypertrophic effects of δPKC and εPKC. PNAS 98: 11114–11119.
57. Brandman R, Disatnik MH, Churchill E, Mochly-Rosen D (2007) Peptides derived from the C2 domain of protein kinase Cε (εPKC) modulate εPKC activity and identify potential protein-protein interaction surfaces. J Biol. Chem. 282: 4113–4123.
58. Toyoda M, Yamazaki-Inoue M, Itakura Y, Kuno A, Ogawa T, et al. (2011) Lectin microarray analysis of pluripotent and multipotent stem cells. Genes Cells 16: 1–11.
59. Okamoto R, Suemori H, Nakatsuji N, Nito S, Kondo Y, et al. (2004) Development of A Novel Measuring Method for Alkaline Phosphatase Activity of Primate Embryonic Stem Cell. Tissue culture research communications : the journal of experimental & applied cell culture research 23: 36.
60. Hayashi Y, Furue MK, Okamoto T, Ohnuma K, Myoishi Y, et al. (2007) Integrins regulate mouse embryonic stem cell self-renewal. Stem Cells 25: 3005–3015.
61. Adewumi O, Aflatoonian B, Ahrlund-Richter L, Amit M, Andrews PW, et al. (2007) Characterization of human embryonic stem cell lines by the International Stem Cell Initiative. Nat. Biotechnol. 25: 803–816.
62. Chia NY, Chan YS, Feng B, Lu X, Orlov YL, et al. (2010) A genome-wide RNAi screen reveals determinants of human embryonic stem cell identity. Nature 468: 316–320.

LETTER TO THE EDITORS

Beware Imposters: MA-1, a Novel MALT Lymphoma Cell Line, is Misidentified and Corresponds to Pfeiffer, a Diffuse Large B-cell Lymphoma Cell Line

To the Editors:

We noted with some anticipation a recent publication in this journal, describing the establishment of a novel mucosa-associated lymphoid tissue (MALT) lymphoma cell line, MA-1 (Kuo et al., 2011). To our knowledge, this would be the first cell line to be successfully established from gastric MALT lymphoma, an unusual extranodal form of B-cell lymphoma. MALT lymphoma has been extensively characterized over the last several decades, but further discoveries are hampered by lack of access to appropriate in vitro models for the disorder (Du, 2007).

Our anticipation was tempered, however, by the knowledge that novel cell lines often do not match up to expectations because of cross-contamination and misidentification. Cultures being handled for prolonged periods—for example, during cell line establishment—can easily be cross-contaminated if cells from another culture are introduced by accident (Capes-Davis et al., 2013). The original culture is almost always overgrown by the imposter cell line, often without the scientist at the microscope being aware of the change. The end result is a misidentified cell line, and a series of publications that relate to the imposter rather than the original tissue, cell type or disease state.

Cell line cross-contamination and misidentification are not new. Publications dating from the 1960s to the present day (Masters et al., 2012) have urged the scientific community to thoroughly characterize novel cell lines, and authenticate cell line stocks used in experimental work. Recently, however, a sustained effort has been made to standardize the methods used to authenticate human cell lines. Short tandem repeat (STR) profiling is now accepted as an effective way to authenticate human cell lines. A Standard has been published by the American National Standards Institute (ANSI), giving protocols and guidelines for STR profiling as applied to cell lines (ANSI/ATCC ASN-0002–2011, 2012). The International Cell Line Authentication Committee (ICLAC) was established following publication of the Standard to increase awareness and provide resources to help address these ongoing problems (Masters et al., 2012).

The MA-1 cell line was analyzed using STR profiling, and its STR profile was published as part of its characterization (Kuo et al., 2011). However, for a cell line to be authenticated, there is a requirement to compare that profile to another sample—preferably from the same donor. Online databases have been developed to allow comparison to other commonly used cell lines, with results made available for this purpose by cell line repositories worldwide (Dirks et al., 2010).

An STR profile for the donor of MA-1 was not made available (Kuo et al., 2011), so we compared the cell line result to several STR profile databases (Dirks et al., 2010). A match was found to the Pfeiffer cell line, held by the American Type Culture Collection (ATCC) and established in 1992 from a patient with non-Hodgkin lymphoma (Gabay et al., 1999). Comparison of the two STR profiles shows 100% match across eight core STR loci and the gender marker amelogenin (Table 1). These loci have been shown to unequivocally authenticate 98% of cell line samples when assessed using a dataset of 2,279 samples from four cell banks (Capes-Davis et al., 2013). The MA-1 cell line was subsequently obtained from the authors and retested at the Leibniz Institute German Collection of Microorganisms and Cell Cultures (DSMZ) with identical results. Unless further stock can be found that corresponds to the original donor, we must conclude that the MA-1 cell line is misidentified and cannot be used as a model for MALT lymphoma.

Laboratories and cell line repositories worldwide are working to characterize existing cell lines, focusing on authentication and disease-specific markers and mutations (Ottaviano et al., 2010). This task is made more difficult by lack of

*Correspondence to: Amanda Capes-Davis, CellBank Australia, Children's Medical Research Institute, Locked Bag 23, Wentworthville, NSW 2145, Australia. E-mail: acapdav@gmail.com

Received 20 February 2013; Accepted 25 June 2013

DOI 10.1002/gcc.22094

Published online 00 Month 2013 in Wiley Online Library (wileyonlinelibrary.com).

© 2013 Wiley Periodicals, Inc.

TABLE 1. STR Profiles, MA-1 and Pfeiffer Cell Lines

Cell line	D5S818	D13S317	D7S820	D16S539	vWA	TH01	AMEL	TPOX	CSF1PO
MA-1 Kuo et al., 2011	10,13	11,12	8,12	12	17,18	9,9.3	X,Y	9	10,11
Pfeiffer ATCC CRL-2632	10,13	11,12	8,12	12	17,18	9,9.3	X,Y	9	10,11

The table lists STR profiles for MA-1 and Pfeiffer. The STR profile for Pfeiffer comes from the ATCC catalogue entry. Eight core STR loci and amelogenin are listed here, as the common loci across these two results; they correspond to the accepted minimum for STR profiling of human cell lines (Capes-Davis et al., 2013). Additional loci for MA-1 can be viewed in the reference, Kuo et al. (2011).

information on the provenance of many cell lines, and lack of donor tissue as a gold standard for comparison. For older cell lines, the date of establishment may be decades in the past and so it may be too late to address these issues. Novel cell lines give us an ongoing opportunity to reduce the impact of imposter cell lines.

Guidelines on characterization of novel cell lines have been developed and should be followed for any published leukemia-lymphoma cell line (Drexler and Matsuo, 1999). To avoid misidentified cell lines in future, we encourage readers establishing novel cell lines to:

1. Set aside donor material (tissue and DNA) to act as a reference for authentication.
2. Generate a baseline STR profile for any human cell line derived from that donor.
3. Compare these baseline STR profiles to the donor and other cell lines. Comparison to other cell lines is possible using online databases (Dirks et al., 2010). In addition to existing databases, a new BioSample database has been developed by the NCBI and is now receiving samples from the scientific community (Masters et al., 2012).
4. Store as many early passages from the culture as feasible—if misidentification is discovered later, it may be possible to return to earlier vials to resuscitate the culture.
5. Keep good records including clinical and culture data so that the provenance of the cell line can be clearly established (Drexler and Matsuo, 1999).
6. Refer to the resources developed by ICLAC for further advice on how to incorporate authentication into everyday culture practice, and guidelines for authenticating human cell lines (Masters et al., 2012).

In the case of the MA-1 cell line, STR profiling has led us to conclude that this cell line is misidentified and cannot be used as a model for MALT lymphoma. Without the publication of its STR profile, the problem with MA-1 would remain undetected. We therefore urge that authentication testing should be adopted more generally, by *Genes, Chromosomes and Cancer* and other journals, as a prerequisite for publishing results using continuous cell lines.

Amanda Capes-Davis*
CellBank Australia – Children's Medical Research Institute, Westmead, New South Wales, Australia

Christine Alston-Roberts,
Liz Kerrigan and
Yvonne A. Reid
American Type Culture Collection (ATCC), Manassas, VA

Tanya Barrett
National Center for Biotechnology Information (NCBI),
National Library of Medicine (NLM),
National Institutes of Health (NIH),
Bethesda MD

Edward C. Burnett and
Jim R. Cooper
Culture Collections Public Health England, Porton Down, UK

R. Ian Freshney
Institute of Cancer Sciences, University of Glasgow, Glasgow, UK

Lyn Healy
UK Stem Cell Bank, National Institute for Biological Standards and Control, Potters Bar, UK

Arihiro Kohara
Japanese Collection of Research Bioresources (JCRB), National Institute of Biomedical Innovation, Osaka, Japan
Christopher Korch
DNA Sequencing and Analysis Core, University of Colorado – Anschutz Medical Campus, Aurora, CO

John R. W. Masters
The Prostate Cancer Research Centre,
University College London, London, UK

Yukio Nakamura
RIKEN BioResource Center,
Cell Engineering Division, Tsukuba, Japan

Raymond W. Nims
RMC Pharmaceutical Solutions,
Longmont, CO

Douglas R. Storts
Promega Corporation, Madison, WI

Wilhelm G. Dirks,
Roderick A. F. MacLeod, and
Hans G. Drexler
Leibniz Institute DSMZ – German
Collection of Microorganisms
and Cell Cultures,
Braunschweig, Germany

REFERENCES

ANSI/ATCC ASN-0002-2011. 2012. Authentication of human cell lines: standardization of STR Profiling. ANSI eStandards Store, Available at: http://webstore.ansi.org/RecordDetail.aspx?sku-ANSI%2fATCC+ASN-0002–2011. last accessed July 17, 2013.

Capes-Davis A, Reid YA, Kline MC, Storts DR, Strauss E, Dirks WG, Drexler HG, Macleod RA, Sykes G, Kohara A, Nakamura Y, Elmore E, Nims RW, Alston-Roberts C, Barallon R, Los GV, Nardone RM, Price PJ, Steuer A, Thomson J, Masters JR, Kerrigan L. 2013. Match criteria for human cell line authentication: Where do we draw the line? Int J Cancer 132:2510–2519.

Dirks WG, MacLeod RA, Nakamura Y, Kohara A, Reid Y, Milch H, Drexler HG, Mizusawa H. 2010. Cell line cross-contamination initiative: An interactive reference database of STR profiles covering common cancer cell lines. Int J Cancer 126:303–304.

Drexler HG, Matsuo Y. 1999. Guidelines for the characterization and publication of human malignant hematopoietic cell lines. Leukemia 13:835–842.

Du MQ. 2007. MALT lymphoma: Recent advances in aetiology and molecular genetics. J Clin Exp Hematop 47:31–42.

Gabay C, Ben-Bassat H, Schlesinger M, Laskov R. 1999. Somatic mutations and intraclonal variations in the rearranged Vkappa genes of B-non-Hodgkin's lymphoma cell lines. Eur J Haematol 63:180–191.

Kuo SH, Weng WH, Chen ZH, Hsu PN, Wu MS, Lin CW, Jeng HJ, Yeh KH, Tsai HJ, Chen LT, Cheng AL. 2011. Establishment of a novel MALT lymphoma cell line, ma-1, from a patient with t(14;18)(q32;q21)-positive Helicobacter pylori-independent gastric MALT lymphoma. Genes Chromosomes Cancer 50:908–921.

Masters JR, Alston-Roberts C, Barrett T, Burnett EC, Cooper JR, Dirks WG, Freshney RI, Healy L, Kerrigan L, Kohara A, Korch C, MacLeod RA, Nakamura Y, Nims RW, Reid YA, Storts DR, Capes-Davis A. 2012. Cell-line authentication: End the scandal of false cell lines. Nature 492:186.

Ottaviano L, Schaefer KL, Gajewski M, Huckenbeck W, Baldus S, Rogel U, Mackintosh C, de Alava E, Myklebost O, Kresse SH, Meza-Zepeda LA, Serra M, Cleton-Jansen AM, Hogendoorn PC, Buerger H, Aigner T, Gabbert HE, Poremba C. 2010. Molecular characterization of commonly used cell lines for bone tumor research: A trans-European EuroBoNet effort. Genes Chromosomes Cancer 49:40–51.

OPEN ACCESS Freely available online

PLOS | ONE

An *In Vitro* ES Cell-Based Clock Recapitulation Assay Model Identifies CK2α as an Endogenous Clock Regulator

Yasuhiro Umemura[1☯], Junko Yoshida[2], Masashi Wada[1], Yoshiki Tsuchiya[1], Yoichi Minami[1], Hitomi Watanabe[3], Gen Kondoh[3], Junji Takeda[2], Hitoshi Inokawa[1], Kyoji Horie[2,4,5*], Kazuhiro Yagita[1,4*☯]

1 Department of Physiology and Systems Bioscience, Kyoto Prefectural University of Medicine, Kyoto, Japan, **2** Department of Social and Environmental Medicine, Osaka University Graduate School of Medicine, Osaka, Japan, **3** Laboratory of Animal Experiments for Regeneration, Institute for Frontier Medical Sciences, Kyoto University, Kyoto, Japan, **4** Precursory Research for Embryonic Science and Technology, Japan Science and Technology Agency, Saitama, Japan, **5** Department of Physiology II, Nara Medical University, Nara, Japan

Abstract

We previously reported emergence and disappearance of circadian molecular oscillations during differentiation of mouse embryonic stem (ES) cells and reprogramming of differentiated cells, respectively. Here we present a robust and stringent *in vitro* circadian clock formation assay that recapitulates *in vivo* circadian phenotypes. This assay system first confirmed that a mutant ES cell line lacking *Casein Kinase I delta* (*CKIδ*) induced ~3 hours longer period-length of circadian rhythm than the wild type, which was compatible with recently reported results using *CKIδ* null mice. In addition, this assay system also revealed that a *Casein Kinase 2 alpha* subunit (*CK2α*) homozygous mutant ES cell line developed significantly longer (about 2.5 hours) periods of circadian clock oscillations after *in vitro* or *in vivo* differentiation. Moreover, revertant ES cell lines in which mutagenic vector sequences were deleted showed nearly wild type periods after differentiation, indicating that the abnormal circadian period of the mutant ES cell line originated from the mutation in the *CK2α* gene. Since *CK2α* deficient mice are embryonic lethal, this *in vitro* assay system represents the genetic evidence showing an essential role of *CK2α* in the mammalian circadian clock. This assay was successfully applied for the phenotype analysis of homozygous mutant ES cells, demonstrating that an ES cell-based *in vitro* assay is available for circadian genetic screening.

Citation: Umemura Y, Yoshida J, Wada M, Tsuchiya Y, Minami Y, et al. (2013) An *In Vitro* ES Cell-Based Clock Recapitulation Assay Model Identifies CK2α as an Endogenous Clock Regulator. PLoS ONE 8(6): e67241. doi:10.1371/journal.pone.0067241

Editor: Shin Yamazaki, University of Texas Southwestern Medical Center, United States of America

Received March 31, 2013; **Accepted** May 15, 2013; **Published** June 28, 2013

Copyright: © 2013 Umemura et al. This is an open-access article distributed under the terms of the Creative Commons Attribution License, which permits unrestricted use, distribution, and reproduction in any medium, provided the original author and source are credited.

Funding: This work was supported in part by PRESTO Program of the Japan Science and Technology Agency (K.Y. and K. H.), and by JSPS KAKENHI Grant Number 23390051 (K.Y.). This work was also supported by the Takeda Science Foundation (K.Y.). The funders had no role in study design, data collection and analysis, decision to publish, or preparation of the manuscript.

Competing Interests: The authors have declared that no competing interests exist.

* E-mail: kyagita@koto.kpu-m.ac.jp (KY); k-horie@naramed-u.ac.jp (KH)

☯ These authors contributed equally to this work.

Introduction

The circadian clock is an intrinsic time-keeping system regulating various physiological functions such as sleep/awake cycle, body temperature and metabolism [1–3]. The core component is the cell-autonomous molecular oscillator comprised of transcriptional-translational feedback loops of clock genes such as *Bmal1*, *Clock*, *Period* (*Per1, 2, 3*) and *Cryptochrome* (*Cry1, 2*) [1]. Two transcription factors CLOCK and BMAL1 transactivate the *Per* genes, *Cry* genes and *Rev-Erbα* via the E-box enhancer elements. Expressed PER and CRY then suppress CLOCK/BMAL1 activity, which results in the cyclic activation of these clock genes [1,4,5]. The *Bmal1* gene also shows cyclic expression but an anti-phasic pattern with E-box driven clock genes because of REV-ERBα cyclically activate the *Bmal1* transcription [6]. In these circadian feedback loops, Casein Kinase I δ/ε (CKIδ/ε) have been known essential central kinases to regulate the stability of PER proteins through their phosphorylation [7–10].

It has been reported that the master pacemaker in the suprachiasmatic nucleus (SCN) develops in the late embryonic stage, and circadian rhythms subsequently appear around birth [11,12]. Recently, our studies using mouse embryonic stem (ES) cells and *in vitro* differentiation culture suggested cell-autonomous development of circadian molecular oscillators in mouse ES cells during differentiation [13,14]. ES cells showed no apparent molecular oscillation, in contrast to somatic cells. However, the circadian oscillation of clock gene reporters became detectable following *in vitro* differentiation. Moreover, reprogramming of differentiated, rhythmic cells into pluripotent stem cells resulted in the loss of circadian oscillation [13]. These results are consistent with the notion that cell-autonomous development of the mammalian circadian clock is coupled with cellular differentiation.

Genetic screening for circadian clock genes has been successfully conducted in mice using chemical mutagenesis [15,16]. Our finding of *in vitro* circadian clock formation through ES cell differentiation provides us with the opportunity to develop a complementary screening system in tissue culture. We recently constructed a homozygous mutant ES cell bank which facilitates phenotypic analysis of various genes in tissue culture [17].

In the present study, we established a highly consistent differentiation protocol and conducted genetic analysis of circadian rhythm using our mutant ES cells. It has been revealed that CKIδ is essential as a central kinase of the mammalian circadian

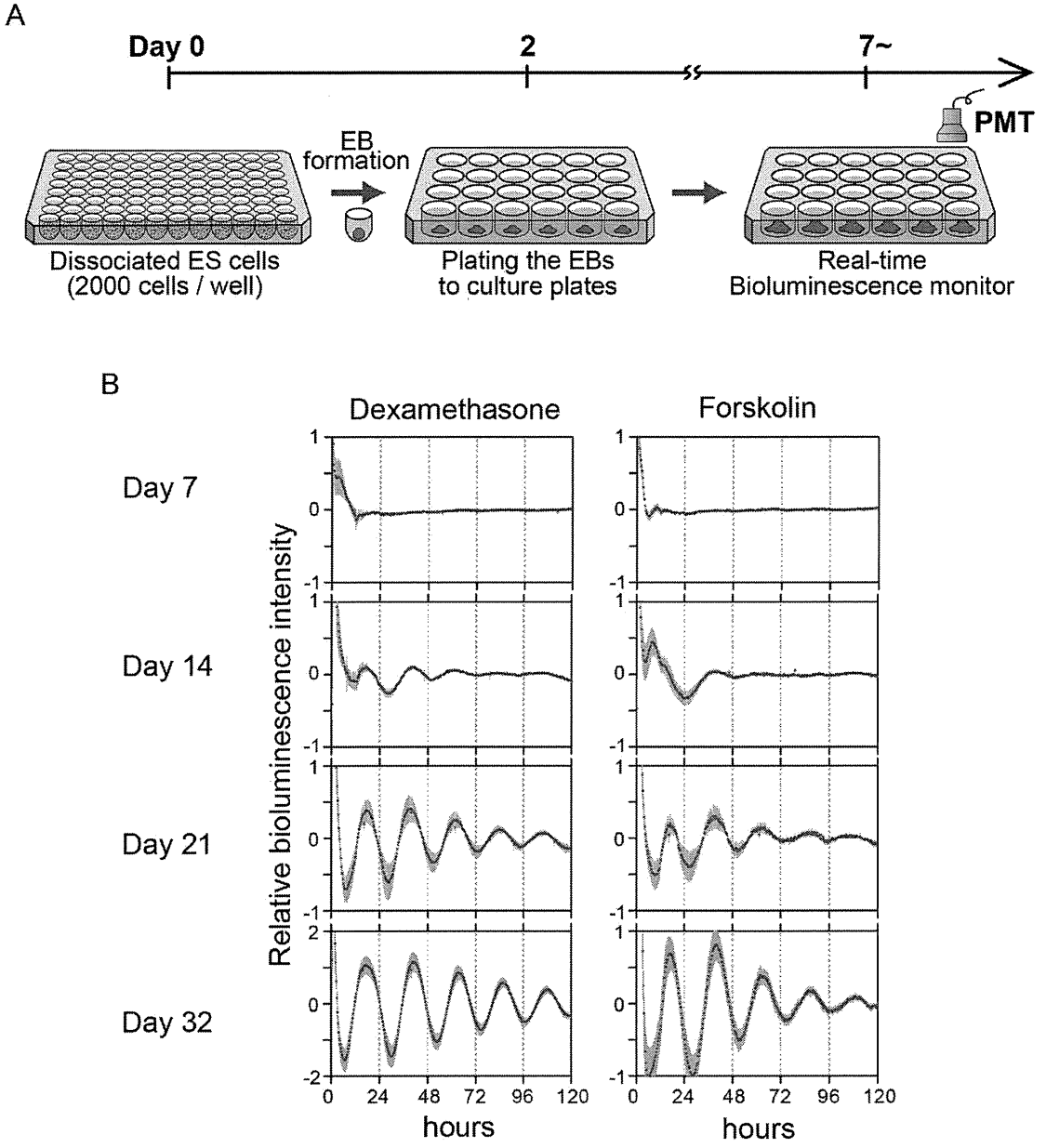

Figure 1. Establishment of *in vitro* circadian clock formation assay system using ES cells. (A) Scheme of the method for developing circadian oscillation *in vitro* via formation of embryoid bodies (EBs). EBs were generated from 2,000 ES cells and were seeded onto low-attachment 96-well plates in differentiating medium without LIF supplementation (see Methods). Two days later, EBs were plated onto gelatin-coated tissue culture 24-well plates (putting one ES onto one well) and cultured for several weeks. Subsequently, bioluminescence in each well was monitored by using PMT-based photon counting. (B) Averaged bioluminescence traces after *in vitro* 7, 14, 21, or 32-day differentiation of ES cells carrying *Bmal1:luc* reporter (*left*, Dexamethasone reset; *right*, Forskolin reset). Data detrended by subtracting a 24-h moving average are means with standard deviation ($n = 24$).
doi:10.1371/journal.pone.0067241.g001

clock [7,8], and that genetic ablation of *CKIδ* results in the lengthening of the circadian period for ~2 hours in mouse embryonic fibroblasts and suprachiasmatic nucleus [18,19]. In this study, we first tested the reliability of our *in vitro* circadian clock formation assay to see whether the definitive features of circadian clock such as temperature compensation and genetically determined phenotypes were correctly recapitulated using wild type ES cell line and homozygous mutant ES cell line lacking *CKIδ* expression.

In addition to CKIδ/ε, Casein Kinase 2 (CK2) has recently also been implicated in circadian clock regulation using genome-wide RNAi screening studies [8,20]. In species other than mammals, CK2 has been revealed to play an essential role for circadian rhythm maintenance [21,22]. However, detailed genetic analysis of *CK2* has been hampered in mammals by embryonic lethality in *CK2* knockout mice. We therefore chose *CK2α* homozygous mutant ES cell line from the homozygous mutant ES cell bank [17] and investigated the effect of *CK2α* deficiency on circadian rhythm.

Materials and Methods

Ethics Statement

All procedures with animals were approved by Kyoto Prefectural University of Medicine Animal Care Committee.

Mutant ES Cells

Mutant ES cell lines for casein kinase I delta (abbreviated as *CKIδ* or *Csnk1d*) and casein kinase 2 alpha subunit (abbreviated as *CK2α* or *Csnk2a1*) were generated by insertional mutagenesis with the retroviral vector as described previously [17]. The vector insertion sites are as follows (mouse genome database mm9, July 2007): *CKIδ*: chromosome 11, position 12,0852,242; *CK2α*: chromosome 2, position 152,053,325.

Cell Culture

Wild type ES cells, genetically mutated ES cell lines (*CKIδ* or *CK2α*), and their revertant ES cells [17] were used for *in vitro* differentiation. These ES cells were cultured on the feeder layer of mitomycin C-treated primary mouse embryonic fibroblasts in ES cell medium (ESM), which contains Glasgow Minimum Essential Medium (G-MEM, Wako) supplemented with 15% fetal bovine serum (FBS, Hyclone), 0.1 mM MEM nonessential amino acids (Nacalai Tesque), 0.1 mM 2-mercaptoethanol (Sigma), 1,000 units/mL of leukemia inhibitory factor (LIF), and 100 units/mL of penicillin–streptomycin (Nacalai Tesque).

To establish ES cells stably expressing *Bmal1:luc* reporter, 3 μg of *Bmal1:luc*-pT2A plasmid with Zeocin™ selection marker [13] and 1 μg of a Tol2 transposase expression vector (pCAGGS-TP) [23] were diluted in 35 μL of ESM and 12 μL of Fugene 6 transfection reagent (Promega) and mixed well. After a 15-min incubation at room temperature, the mixture was added to 2.5×10^5 ES cells. The cells were selected with 100 μg/mL Zeocin™ (Invitrogen).

In vitro Differentiation

After ES cells were trypsinized, feeder cells were removed by incubating the cell suspension on a gelatin-coated 35-mm or 60-mm culture dish for 20 min at 37°C with 5% CO_2. Embryoid bodies (EBs) were generated by harvesting the 2,000 cells and seeding them onto low-attachment 96-well plates (Lipidure Coat, NOF) in differentiating medium without LIF supplementation (EFM), that is high glucose Dulbecco's modified Eagle medium (DMEM, Nacalai Tesque) containing 12% FBS, 1 mM sodium pyruvate (Nacalai Tescque), 0.1 mM nonessential amino acids, GlutaMax™-I (Invitrogen), 0.1 mM 2-mercaptoethanol (Sigma), and 100 units/mL penicillin-streptomycin. Two days later, EBs were plated onto gelatin-coated tissue culture 24-well plates (put one EB into one well) and grown for several additional weeks **(see Fig. 1A)**.

Preparation of MEFs Derived from Chimeric Embryo

Chimeric embryos were generated from homozygous *CKIδ* or *CK2α* mutant ES cell lines and their parental (wild type) ES cell line by injection into C57BL/6 x DBA/2 F1 hybrid blastocysts. Chimeric embryos were collected at E13.5. After removal of the heads and visceral tissues, the remaining bodies were washed in fresh PBS and minced and the isolated cells were maintained in EFM.

Real-time Bioluminescence Analysis

For real-time bioluminescence analysis of the cells seeded in 24-well black plates, the medium was replaced with EFM containing 0.2 mM luciferin (Promega) and 10 mM HEPES without phenol red. Synchronization was performed using 100 nM of dexamethasone or 10 μM of forskolin for 1 hour. The plates were set on the turntable of house-made 24-PMT head type real-time monitoring equipment [24]. The bioluminescence from each well was counted for 1 minute in every 20 minutes.

Data Analysis

Period lengths of bioluminescence rhythms were estimated by RAP software (CHURITSU, Nagoya, Japan) using the cosinor method and based on Fourier analysis, specific for circadian rhythms [25]. Strength of rhythmicity was defined by spectral analysis (FFT relative power) as the relative spectral power density at the peak within the range of 20–28 hr [26]. The FFT analysis was applied to the whole five days excluding the first 12 h of data. For raster plots, bioluminescence-intensity data were detrended by subtracting a 24-h moving average, normalized for amplitude, and then color coded with red (higher than average) and green (lower than average). Plots were constructed using TreeView [27].

Statistical Analysis

Statistical differences were evaluated using one-way ANOVA followed by a Bonferroni post hoc test. All statistics were calculated using GraphPad Prism version 5.0 software.

Isolation of Revertant Clones

Revertant clones were isolated by transfecting homozygous clones with a FLPo expression vector followed by PCR screening for recombination events as described previously [17]. The following PCR primers at the flanking regions of the vector insertion sites were used:

Casein kinase 1δ : 5′-tgc cat gga gct gag ggt cgg gaa cag gta-3′ and 5′-tgc ggg gat gcc gaa cgt cca ct-3′.

Casein kinase 2α : 5′-gag atg tgg tag aaa gag aaa ggt tg-3′ and 5′-cct gtc acc ttt tca caa tac ttc tt-3′.

Quantitative RT-PCR

MEF feeder cells were removed by plating the culture on a gelatin-coated dish for 20 min and transferring unattached ES cells onto a fresh dish. ES cells were harvested in the Isogen reagent (Nippon Gene) and the total RNA was extracted according to the manufacturer's instructions. Power SYBR Green PCR Master Mix (Applied Biosystems) was used for real time PCR. Transcription levels were determined in triplicate reactions after normalization to 18S ribosomal RNA. Quantitative RT-PCR analysis was performed with a StepOnePlus real-time PCR system (Applied Biosystems). The amplification protocol comprised an initial incubation at 95°C for 2 min and 40 cycles of 95°C for 30 s and 60°C for 30 s, followed by dissociation-curve analysis to confirm specificity. Primer sequences are shown below:

Casein kinase 1δ Forward 5′-atc gcc aag gct tct cct-3′.

Casein kinase 1δ Reverse 5′-cca cga gtg gct gga ttc-3′.

Casein kinase 2α Forward 5′-tca gca gcg cca ata tga-3′.

Casein kinase 2α Reverse 5′-acc tct gct cag gca tca-3′.

Results

In vitro ES Cell-based Circadian Clock Formation Assay

To evaluate the effect of the mutations on the *in vitro* development of the circadian clock in ES cells, we improved our ES cell differentiation protocol and established a method for robust, reproducible and stringent circadian clock formation. Briefly, we first cultured dissociated 2,000 ES cells for two days in round-bottom low-attachment 96-well plates to allow formation of

the embryoid body (EB). We subsequently transferred one EB into one well of 24-well plates for differentiation (**Figure 1A**). To monitor development of circadian oscillation, we used a wild-type (WT) ES cell line stably transfected with a *Bmal1:luc* reporter. Whereas no circadian oscillation of *Bmal1:luc* reporter bioluminescence was detected even after Dexamethasone (Dex) or Forskolin (FSK) synchronization stimuli in an undifferentiated state, weak circadian bioluminescence first appeared in cultures after 14 days but rapidly dampened (**Figure 1B**). The bioluminescence oscillation become more robust on day 21 and reached maximum amplitude on day 32 (**Figure 1B**). In addition, all examined samples represented robust circadian clock oscillation and stringent reproducibility for quantitative analysis (**Figure S1**). Moreover, the induced rhythms showed temperature compensation (**Figure S2**), indicating the canonical biological nature of the circadian clock.

Casein Kinase 1δ and Casein Kinase 2 Homozygous Mutant ES Cells

We recently constructed a homozygous mouse mutant ES cell bank using promoter trap vectors for insertional mutagenesis [17]. Currently, the bank has around 200 homozygous mutant ES cell lines and 2,000 heterozygous mutant ES cell lines. Database search of the mutant bank for the circadian period mutant identified two homozygous mutant ES cell lines, harboring mutation in *CKIδ* and *CK2α* respectively. We confirmed that homozygous mutation abolished expression of the *CKIδ* and *CK2α* gene (**Figure 2A and D**). As a control, we obtained revertant ES cell lines which regained *CKIδ* and *CK2α* expression respectively (**Figure 2B–D**) [**17**].

Evaluation of Developed Circadian Clock Rhythmicity from Mutant ES Cell Lines

Using this *in vitro* differentiation culture method, *CKIδ* and *CK2α* homozygous mutant ES cells were differentiated *in vitro* and *Bmal1:luc* bioluminescence oscillation was observed. Similar to the WT ES cells (**Figure 3A left panels**), *CKIδ* and *CK2α* mutant ES cells developed circadian oscillation in a differentiation culture (**Figure 3A middle and right panels**). Heat map plots (**Figure S3**) and quantitative Fast Fourier transformation (FFT) - relative power analysis (**Figure 3B left panel**) also indicated that circadian rhythmicity and amplitude developed progressively and reached the highest levels of power at around day 28 during the ES cell differentiation *in vitro*. These results suggest quantitative analysis of circadian clock formation would be possible after 28 days of differentiation.

We next conducted in-depth analyses of the *CKIδ* and *CK2α* homozygous mutations on cellular circadian rhythmicity. After 28 days in the differentiation culture, bioluminescence monitoring was performed for five days. The results revealed that the *CKIδ* and *CK2α* deficient cells exhibited significantly lengthened circadian periods compared with WT and revertant cells (**Figure 4A and D**). In addition, the period distribution of induced circadian clocks in *CKIδ* and *CK2α* mutants showed a slightly wider range than WT and revertant cells (**Figure 4B and E**). The average period length of *CKIδ* and *CK2α* mutant cells were about 3.0 and 2.5 hours longer than that of WT, respectively (**Figure 4C and F**). In contrast, revertant lines of both mutants showed WT-like period lengths (**Figure 4C and F**).

Genotype Dependent Effect on Circadian Period-length Observed in Mutant ES Cell-derived Embryonic Fibroblasts

To investigate whether the abnormal period-length observed in *in vitro* differentiation culture of mutant ES cells recapitulates the characters of circadian clock developed *in vivo*, we generated chimeric mice by injecting WT and mutant ES cells into BDF1 blastocysts. Since *CKIδ* knock-out mice were perinatal lethal and *CK2α* knock-out mice were embryonic lethal, we prepared MEFs from E13.5 chimera embryos instead of mice (**Figure 5A**). In these MEFs, we were able to specifically monitor bioluminescence originated from ES cell lines, because host embryos are incapable of expressing the bioluminescence marker. In addition, it has been revealed that fibroblast oscillators are not influenced by the circadian properties of neighboring cells [28]. Therefore we analyzed the bioluminescence oscillation from the mixture of MEFs composed of host-derived and ES cell-derived MEFs after three passages from embryo dissociation. PMT-based bioluminescence monitoring revealed that both *CKIδ* and *CK2α* mutant ES cell-derived MEFs displayed lengthened periods compared with WT ES cell-derived MEFs (**Figure 5B**). Quantitative analysis confirmed significantly longer periods in *CKIδ* and *CK2α* mutant MEFs (**Figure 5C**). *CKIδ* mutant MEFs showed 24.3 hour period, nearly two hours longer than WT ES MEFs (**Figure 5D upper and middle panels**). On the other hand, *CK2α* mutant MEFs showed divergent period distribution (**Figure 5D lower panel**). Since this *CK2α* mutant ES cell line abolished its gene expression, the observed phenotypes such as longer and variable periods may be characteristic of *CK2α* deficient cells. The reason for the divergent period-length of these cell was not uncertain; the loss of *CK2α* may have affected the circadian clock development in chimeric mice embryos with some different mechanisms from *CKIδ*. To our knowledge, this is the first direct genetic evidence showing the effect of *CK2α* deficiency on circadian clocks in mammalian peripheral cells.

Discussion

It has been revealed that CKIδ plays a distinct role in mammalian circadian clock as a central kinase phosphorylating clock proteins [7–9]. In this study, the *in vitro* circadian clock formation assay revealed that *CKIδ* deficient ES cells developed circadian clock oscillation with a ~ 3 hours longer period-length than WT, and these results are consistent with previously reported circadian phenotypes in MEFs and SCN from *CKIδ* knock-out mice [8,18,19]. Moreover, WT and revertant ES cells with normal *CKIδ* gene expression exhibited comparable circadian periods (**see Figure 4A, B and C**), suggesting *in vitro* clock formation assay in ES cells faithfully reproduce the genetically determined circadian rhythms in mammals. In addition, the developed circadian rhythm from ES cells after *in vitro* differentiation culture exhibited temperature compensation (**see Figure S2**). These findings revealed that the *in vitro* circadian clock formation assay using ES cells exactly recapitulated the circadian clock phenotype (at least in cellular or tissue level) before making mice.

We also demonstrated that *CK2α* deficient ES cells developed at an approximately 2.5 hours longer period-length. The role of *CK2α* in circadian oscillation has been implicated from RNAi-mediated knock-down and/or chemical inhibition of CK2 [20,29–31]. However, off-target effects cannot in general be excluded in RNAi and a chemical inhibitor. Although off-target effects could also accompany gene trap approach, isolation and characterization of revertant (Figure 2 and 4) would help evaluate this possibility. Furthermore, the gene knockout study of *CK2α* has

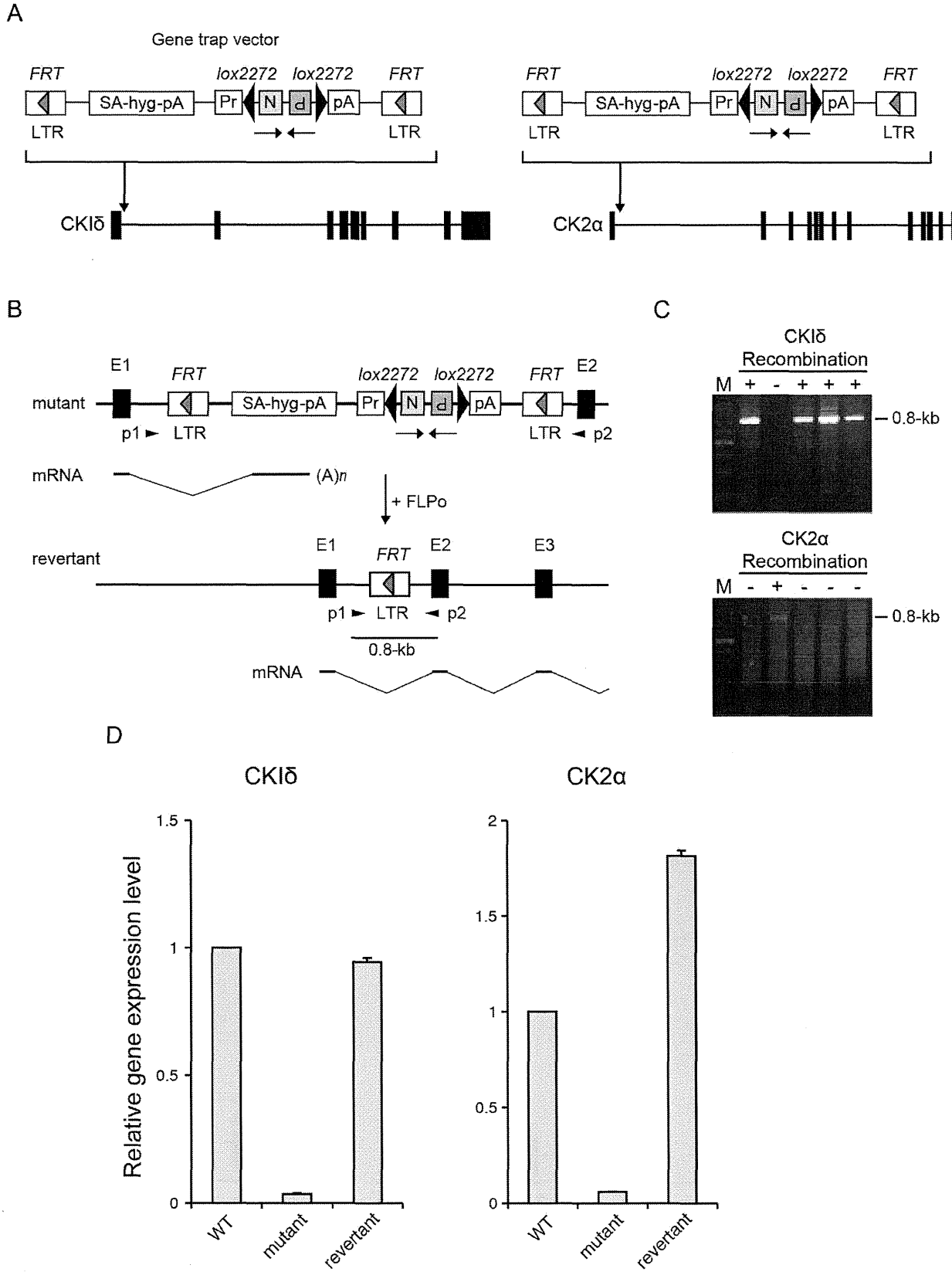

Figure 2. Characterization of *CKIδ* and *CK2α* homozygous mutant ES cell clones and their revertant clones. (A) Design of the gene trap vector and its insertion sites in *CKIδ* and *CK2α* homozygous mutant ES cell clones. SA, splice acceptor; hyg, hygromycin-resistance gene; pA, polyadenylation signal; Pr, phosphoglycerate kinase-1 promoter; N, neomycin-resistance gene; P, fusion gene comprised of the puromycin-resistance gene and the herpes simplex virus thymidine kinase gene; LTR, long terminal repeat. Horizontal arrows below the gene trap vector indicate

orientation of the N and P drug resistance genes. (B) Schematic representation of the removal of mutagenic vector sequence after FLPo/FRT recombination. Recombination events were identified by PCR primers (p1 and p2) at the flanking region of the vector insertion sites. Removal of vector sequences regenerate wild type transcripts in the revertant allele. Note that the size of the gene trap vector, exons, introns are not to scale. E, exon. (C) PCR screening for FLPo/FRT recombination events. Note that PCR product was not detected in non-recombinant clones because of the large intervening vector sequence between primers. M, 100-bp DNA ladder. (D) Relative expression level of *CKIδ* and *CK2α* mRNA in wild type, mutant and revertant ES cells. Error bars show SEM (n = 3).
doi:10.1371/journal.pone.0067241.g002

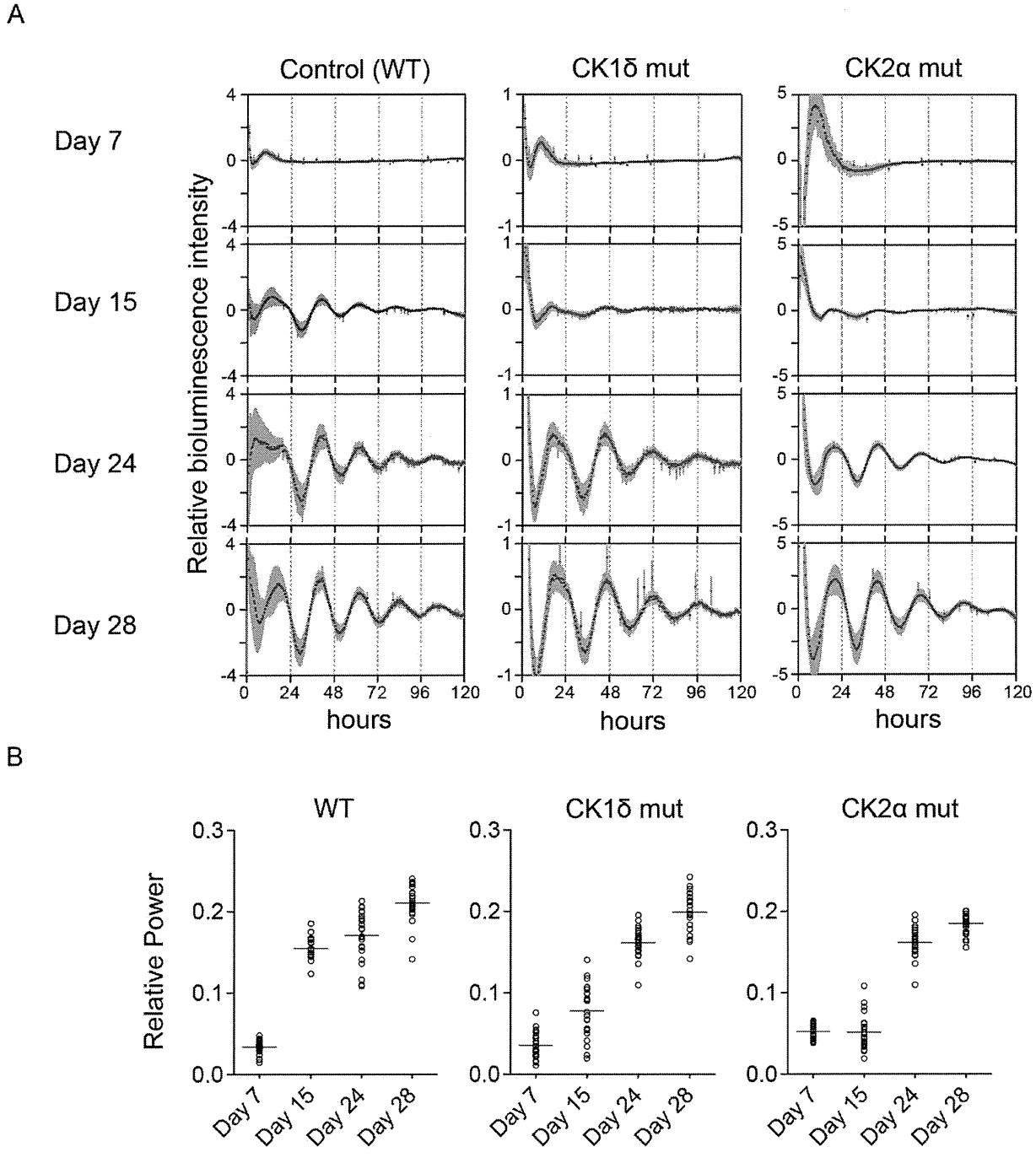

Figure 3. Development of mammalian circadian rhythm by using homozygous mutant ES cells. (A) Averaged bioluminescence traces after *in vitro* 7, 15, 24, or 28-day differentiation of ES cells carrying *Bmal1:luc* reporter (*left*, wild type ES cells (WT); *middle*, *CKIδ* mutant ES cells; *right*, *CK2α* mutant ES cells). Data detrended by subtracting a 24-h moving average are means with standard deviation ($n = 24$). (B) FFT spectral power analysis of bioluminescences of *in vitro* differentiated ES cells (7, 15, 24, or 28-day). Bars indicate mean values ($n = 24$). One circle represented *in vitro* differentiated ES cells from a single EB.
doi:10.1371/journal.pone.0067241.g003